Fibroblast growth factor 13 regulates glioma cell invasion and is important for bevacizumab-induced glioma invasion

Authors:

Yoshihiro Otani 1), Tomotsugu Ichikawa 1), Kazuhiko Kurozumi 1), Satoshi Inoue 2), Joji Ishida 1), Tetsuo Oka 1), Toshihiko Shimizu 1), Yusuke Tomita 1), Yasuhiko Hattori 1), Atsuhito Uneda 1), Yuji Matsumoto 1), Hiroyuki Michiue 3), Isao Date 1)

Departmental and institutional affiliations:

1) Department of Neurological Surgery, Okayama University Graduate School of Medicine, Dentistry, and Pharmaceutical Sciences, Okayama, Japan

2) Department of Neurosurgery, Okayama City Hospital, Okayama, Japan

3) Department of Physiology, Okayama University Graduate School of Medicine, Dentistry, and Pharmaceutical Sciences, Okayama, Japan

Running Title:

FGF13 regulates glioma invasion.

Corresponding author contact information:

Name: Tomotsugu Ichikawa

Address: 2-5-1 Shikata, Kita-ku, Okayama 700-8558, Japan

Phone number: +81-86-235-7336

Fax number: +81-86-227-0191

E-mail address: tomoichi@cc.okayama-u.ac.jp

Accession numbers:

The accession number for the gene expression data reported in this paper is GSE88740.

Funding:

This study was supported by grants-in-aid for Scientific Research from the Japanese Ministry of Education, Culture, Sports, Science, and Technology to T.I. (No. 22591611; No. 25462261) and K.K. (No. 23592125; No. 26462182).

Abstract:

Glioblastoma have the poorest prognosis, and is characterized by excessive invasion and angiogenesis. To determine the invasive mechanisms, we previously used two glioma cell lines (J3T-1 and J3T-2) with different invasive phenotypes. The J3T-1 showed abundant angiogenesis and tumor cell invasion around neovasculature, while J3T-2 showed diffuse cell infiltration into surrounding healthy parenchyma. Microarray analyses were used to identify invasion-related genes in J3T-2 cells, and the expressed genes and their intracellular and intratumoral distribution patterns were evaluated in J3T-2 cell lines, human glioma cell lines, human glioblastoma stem cells, and human glioblastoma specimens. To determine the role of the invasion-related genes, invasive activities were evaluated *in vitro* and *in vivo*. Fibroblast growth factor 13 (FGF13) was overexpressed in J3T-2 cells compared to J3T-1 cells, and in human glioma cell lines, human glioblastoma stem cells, and human glioblastoma specimens, when compared to that of normal human astrocytes. Immunohistochemical staining and the RNA-seq (sequencing) data from the IVY Glioblastoma Atlas Project showed FGF13 expression in glioma cells in the invasive edges of tumor specimens. Also, the intracellular distribution was mainly in the cytoplasm of tumor cells and colocalized with tubulin. Overexpression of FGF13 stabilized tubulin

dynamics *in vitro* and knockdown of FGF13 decreased glioma invasion both *in vitro* and *in vivo* and prolonged overall survival of several xenograft models. FGF13 was negatively regulated by hypoxic condition. Silencing of FGF13 also decreased *in vivo* bevacizumab-induced glioma invasion. In conclusion, FGF13 regulated glioma cell invasion and bevacizumab-induced glioma invasion, and could be a novel target for glioma treatment.

Keywords:

Fibroblast growth factor 13, glioma, invasion, microtubule, bevacizumab

Introduction

Glioblastoma has one of the poorest prognosis of intracranial tumors. Despite advances in basic and clinical studies, the outcomes of the patients remain poor, with the median survival time being 14.6 months (1). The causes of glioblastoma poor prognoses include its typical aggressive invasiveness, high angiogenesis, and proliferation. Recently, antiangiogenic treatments were used in clinical trials, however, no trials showed prolongation of overall survival (2) (3). Piao et al. reported that anti-vascular endothelial growth factor (anti-VEGF) therapy induced more invasive and treatment-resistant phenotypes (4). We have also shown that antiangiogenic therapy induced invasion in the orthotopic glioma models (5) (6).

Glioma cells often migrate along brain structures including blood vessels and white matter tracts (7). We have previously established two novel invasive glioma cell line models, J3T-1 and J3T-2 (8) (9) that mimicked the angiogenic and invasive phenotypes of human glioblastoma (10). The J3T-1 model formed vascular rich tumor masses, and in adjacent normal brain tissues, the tumor cells clustered around the neovasculature. In contrast, the J3T-2 model formed tumor masses with the invasion of single cells into the normal brain parenchyma along white matter tracts. Previously, we reported that annexin A2, which was abundantly expressed in the J3T-1 model, was involved in angiogenesis-dependent growth

of glioma (11).

We further showed the presence of the newly identified invasion-related gene, fibroblast growth factor 13 (FGF13) [also named fibroblast growth factor homologous factor 2 (FHF2)], a member of the FGF family, in the invasive J3T-2 glioma model. Recent studies showed that FGF13 was widely distributed in the developing brain (12), was involved in neural differentiation in early development of *Xenopus* (13), and neural migration as a microtubule stabilizing protein (14). FGF13 had two alternative splicing forms: FGF13A that contained a nuclear localizing signal (NLS), and FGF13B that lacked the NLS. Nishimoto et al. reported that FGF13 was increased by SoxD and was involved in the activation of the MEK5-ERK5 pathway in neuronal development (13). FGF13B regulated tubulin dynamics and was involved in neuronal motility (14).Currently, many studies have shown that microtubules appear in glioma and that tumor cell migration and invasion required dynamic reorganization of the cytoskeleton, including actin and microtubules (15, 16). As a result, microtubules have emerged as novel treatment targets to prevent tumor cell motility and invasion (17).

In this study, we showed that FGF13 was highly overexpressed in glioma and the silencing of FGF13 expression reduced glioma cell invasion *in vitro* and *in vivo,* thereby regulating microtubule dynamics. Moreover, bevacizumab-induced glioma invasion was impaired by

knockdown of FGF13.

Results

FGF13 was highly expressed in the invasive glioma model, in various human glioma cell lines, and in human glioma stem cells.

To investigate the difference of invasive ability, the difference of gene expression profiles between J3T-1 and J3T-2 cells were analyzed using microarray data (Supplementary Fig. 1A). Gene Ontology (GO) enrichment analysis using these significantly regulated genes were performed (Table. 1 and 2). GO enrichment analysis of J3T-2 revealed that up-regulated genes in J3T-2 were mostly related to microtubule ($p = 0.011$) and cytoskeletal protein expressing ($p = 0.025$). Among the genes in the microarray data involved in microtubule and cytoskeleton dynamics, FGF13 was overexpressed by 26.0-fold in J3T-2 cells compared to that of the J3T-1 cells. Then, we performed quantitative reverse transcription-polymerase chain reaction (qRT-PCR) assays to confirm the reliability of the results from microarray analyses and determined that the relative expression levels of FGF13 in J3T-2 cells were significantly elevated by 14.8-fold ($p < 0.01$) compared with that of the J3T-1 cells (Supplementary Fig. 1B).

Next, we screened FGF13 mRNA levels in several human glioma cells by using qRT-PCR. The U87ΔEGFR, U251, and LNZ308 cells showed higher expression of FGF13 than that of the normal human astrocyte (NHA) cells, and were approximately 14.7 times, 2.6 times and 4.1 times greater, respectively. Furthermore, the human glioblastoma-derived cancer stem cells (MGG8 and MGG23) that showed a diffusely invasive phenotype, like the J3T-2 (18) cells, also expressed higher FGF13 than that of the NHA cells (41.7 times and 1.91 times, respectively, $p < 0.05$).

The expression of FGF13 protein was dominant in the cytoplasm in glioma cell lines and human glioma specimens, and FGF13 positive glioma cells were located in the invasive edge.

Immunofluorescent staining of J3T-2 cells showed FGF13 (FGF13B) mainly localized in the cytoplasm (Fig. 1A). Next, we also performed immunohistochemical staining of human specimens. In normal brain tissues, FGF13 was mainly expressed in the nucleus of neurons (Fig. 1B). However, in glioblastoma patient specimens, FGF13 protein was dominant in the cytoplasm (Fig. 1C). The relative expression level of FGF13 mRNA and protein in human glioblastoma specimens were significantly correlated ($p = 0.016$, Fig. 1D). Western blotting

also showed FGF13B protein levels were higher than that of FGF13A in human glioblastoma specimens (Fig. 1E) and glioma cell lines (Fig. 2B). At the invasive edge, most tumor cells expressed FGF13 in the cytoplasm (Fig. 1C, right panel), however, in the tumor core, the number of FGF13 positive cells varied in each patient (Fig. 1C, left panel). The percentage of FGF13 positive tumor cells in the tumor core was 12.4%; however the percentage was markedly increased in the invasive edge of the glioblastoma (44.6%) ($p < 0.01$, Fig. 1F). Data from the IVY Glioblastoma Atlas Project also showed that FGF13 was more expressed in the area of both the leading edge and infiltrating tumor than in the cellular tumor, perinecrotic zone, hyperplastic blood vessels, and microvascular proliferations (glioblastoma.alleninstitute.org) (Fig. 1G). Immunohistochemistry revealed that the microenvironment cells like endothelial cells and macrophages did not express FGF13 (Supplementary Fig. 2). We analyzed glioblastoma data from the Cancer Genome Atlas (TCGA) project and we found that FGF13 was more expressed in proneural and neural subtypes than in classical and mesenchymal types (Fig. 1H). For the FGF13 expression based on glioma subtypes, data were analyzed using the Project Betastatis webpage (www.betastasis.com). Low grade glioma also exhibited FGF13 (Supplementary Fig. 3).

Silencing of FGF13 reduced the *in vitro* migration and invasion activity.

To address the role of FGF13 in glioma, we examined the effect of FGF13 knockdown on cell migration and invasion. The siRNA silencing of FGF13 expression reduced FGF13 mRNA expression in J3T-2 cells, and both FGF13 mRNA (Fig 2A) and protein levels (Fig. 2B) in U87ΔEGFR, U251, and LNZ308 cells ($p < 0.05$; Fig. 2A and B). Transwell assays showed that silencing of FGF13 significantly reduced the migration of J3T-2 cells ($p < 0.05$; Fig. 2C and D) and decreased the migration activity of U87ΔEGFR, U251 and LNZ308 cells ($p < 0.05$; Fig. 2C and D). Matrigel invasion assay also confirmed that silencing of FGF13 significantly reduced the invasion of J3T-2 and U87ΔEGFR ($p < 0.05$; Supplementary Fig. 2). In contrast, silencing FGF13 did not affect the migration and invasion of A172 and Gli36Δ5 cells (Supplementary Fig 4A, B and D) that expressed FGF13 at lower levels than that of the NHA cells (Supplementary Fig. 4C).

Although the regulation of microtubules is usually involved in mitotic cell division in both normal and cancer cells, the WST-1 cell viability assay showed FGF13 did not alter glioma cell viability ($p = 0.359$, 0.742, 0.899, and 0.37 in J3T-2, U87ΔEGFR, U251, and LNZ308 cells, respectively; Fig. 2E). Furthermore, FGF13-silenced cells did not indicate

the increase of apoptosis ($p = 0.82$, 0.86, 0.70, and 0.62 in J3T-2, U87ΔEGFR, U251, and LNZ308 cells, respectively; Supplementary Fig. 5). We also evaluated whether knockdown of FGF13 alter cell morphology. However, silencing of FGF13 did not significantly change cell morphology (Supplementary Table 1 and 2).

Silencing of FGF13 expression reduced the invasion and prolonged the survival time in xenograft glioma models bearing J3T-2 or human glioblastoma-derived cancer stem cells.

To investigate the role of FGF13 in the xenograft glioma model, we generated J3T-2, MGG8 and MGG23 cells that had reduced FGF13 expression, using a lentivirus vector encoding a short hairpin RNA (shRNA) against canine or human FGF13. The lentivirus-mediated shRNA reduced the relative FGF13 mRNA expression in J3T-2, MGG8, and MGG23 cells ($p < 0.05$; Fig. 3A, Fig. 4A and Supplementary Fig. 6A). The J3T-2, MGG8 or MGG23 cells expressing FGF13 shRNA or non-targeting shRNA (scramble shRNA) were transplanted into the brain of the athymic mice or the severe combined immunodeficiency (SCID) mice, respectively.

To determine the invasive activity of J3T-2 cells, tissue slices were stained with anti-vimentin antibody that reacted with canine but not mouse. Histological examination showed J3T-2 cells transfected with lentivirus encoding scramble shRNA (J3T-2 scramble shRNA; Fig. 3B and C) gradually migrated from the tumor center to the surrounding normal brain tissue and the edge of tumor. In contrast, the J3T-2 cells transfected with lentivirus encoding FGF13 shRNA (J3T-2 FGF13 shRNA) showed less invasive activity into normal brain than did the J3T-2 scramble shRNA cells and the edge of the tumor was clear of invasive cells (Fig. 3B and C). Knockdown of FGF13 did not affect the MIB-1 labeling index ($p = 0.81$; Fig. 3D and E) and the number of apoptotic cells ($p = 0.84$, Fig. 3F). The number of vessels in the tumor was also evaluated, however, there was no difference between the J3T-2 scramble shRNA and J3T-2 FGF13 shRNA samples ($p = 0.51$, Fig.3G, H). The percentage survival of the J3T-2 FGF13 shRNA treated samples was significantly greater than that of the J3T-2 scramble shRNA treated samples (median survival = 59.5 versus 49 days, respectively; $p = 0.0015$, Fig. 3I).

We also investigated the role of FGF13 in glioma invasion using MGG8. Immunohistochemical examination of MGG8 showed these glioma cells spread from the injection site to the adjacent normal brain, like J3T-2 cells, and invaded along the corpus

callosum. Invasion activity was assessed from the number of tumor cells in the ipsilateral or contralateral cerebral cortex. There was a significant reduction of glioma cells invading into the cerebral cortex with MGG8 cells transfected with lentivirus encoding FGF13 shRNA (FGF13 shRNAs #1, #2; Fig. 4B and C) compared with MGG8 cells transfected with lentivirus encoding scrambled shRNA (scramble shRNA; Fig. 4B and C) ($p < 0.01$). However, knockdown of FGF13 did not affect the number of apoptotic MGG8 cells ($p = 0.71$) (Fig. 4D), cell proliferation ($p=0.85$), and angiogenesis ($p=0.46$) *in vivo*. Kaplan-Meier survival analysis resulted in the improvement of overall survival in the MGG8 FGF13 shRNA #1, #2 injected animals (median survival = 61, 61.5 versus 55.5days, respectively; $p < 0.02$, Fig. 4E). Knockdown of FGF13 in MGG23 also significantly impaired glioma invasion and prolonged OS as well as MGG8 (Supplementary Fig. 6B, C, and F).

FGF13B regulated microtubule dynamics and expression of FGF13 was negatively regulated by hypoxic conditions.

To clarify the functional mechanism of FGF13 in glioma invasion, we focused on the interactions between FGF13 and tubulin dynamics in glioma. Immunohistochemical

staining showed that FGF13 was dominant in the cytoplasm of J3T-2 and colocalized with tubulin (Fig. 5A). Next, we isolated the fraction of soluble tubulin (tyrosinated tubulin; Tyr-tubulin) and insoluble tubulin (acetylated tubulin; Ace-tubulin) from A172 cells transfected with the FGF13B plasmid or untransfected cell and treated with dimethyl sulfoxide (DMSO) or nocodazole, a microtubule destabilizer. The Tyr-tubulin or Ace-tubulin are markers for dynamic or stable microtubules, respectively. Western blotting showed Ace-tubulin in normal A172 was decreased after treatment with nocodazole. However, FGF13B restored the level of Ace-tubulin in A172 cells treated with nocodazole (Fig. 5B). These results showed that FGF13B colocalized with tubulin and could stabilize the microtubule structures. We assessed the role of hypoxic conditions as a mechanism of affecting FGF13 expression. FGF13-positive cells are dominant in the leading edge of tumors compared with the tumor core where hypoxic conditions exist. Western blotting of U87 Δ EGFR and U251 confirmed that hypoxic condition negatively regulated FGF13 expression (Fig. 5C). Tumor cells cultured with 1% O_2 or in medium containing deferoxamine mesylate showed the significant decrease of FGF13 expression (Fig. 5C and Supplementary Fig. 7).

Silencing of FGF13 altered bevacizumab-induced glioma invasion.

Recently, bevacizumab has been used for glioblastoma treatment and shows benefits in progression-free-survival (PFS). However, bevacizumab was reported to induce invasion and this may lead to failures of prolongation of overall-survival (OS). We therefore investigated whether FGF13 also regulated bevacizumab-induced glioma invasion.

First, we evaluated the expression of FGF13 after bevacizumab treatment in human glioma cell lines (Fig. 6A, Supplementary Fig. 8A and B), and human glioblastoma specimens (Fig. 6B and C), and found that the FGF13 expression was not altered after bevacizumab treatment. Western blotting of U87ΔEGFR and U251 showed almost the same expression level of FGF13 in all samples (Fig. 6A, Supplementary Fig. 8A, and B). We analyzed the FGF13 mRNA expression in five patients who had both pre- and post-bevacizumab specimens using a previously published microarray data (19). No changes in FGF13 expression occurred after bevacizumab resistance (Fig. 6C, p=0.7278). Immunohistochemistry of FGF13 in our cohort also confirmed these data (Supplementary Fig. 8E).

Next, we evaluated the role of FGF13 on bevacizumab-induced glioma invasion *in vitro* and *in vivo* using our previously reported bevacizumab-induced glioma invasion model (6). In vitro, double chamber assays showed that bevacizumab treatment significantly induced

glioma cell invasion, however, silencing of FGF13 decreased its invasion ability in both U87ΔEGFR and U251 cells (Supplementary Fig. 8C and D). We generated U87ΔEGFR cells expressing FGF13 shRNA or scramble shRNA (Fig. 6D) and transplanted each cell type *in vivo* into the brain of athymic mice. These mice were treated with either phosphate-buffered saline (PBS) or bevacizumab. Mice in the PBS-treated group showed tumor masses with well-defined borders (Fig. 6E). However, in the bevacizumab-treated group, tumor cell invasion into surrounding normal tissues was induced and the tumor surface became irregular. We evaluated the depth of tumor invasion from the border of the tumor mass to the invaded cells. In U87ΔEGFR expressing scramble shRNA treated with bevacizumab, the mean depth of tumor invasion was 222.7 ± 34.9 μm. However, the depth of tumor invasion in the U87ΔEGFR expressing FGF13 shRNA samples treated with bevacizumab was remarkably decreased (mean, 111.9 ±16.8 μm, $p < 0.05$; Fig. 6E and F, Supplementary Fig. 8F and 8G). These results demonstrated that FGF13 was also involved in bevacizumab-induced glioma invasion.

Discussion

In the present study, our findings suggested that FGF13 regulated microtubule dynamics and was involved in glioma invasion *in vitro* and *in vivo*. FGF13-related invasion was observed in both glioma non-stem cells and glioma stem cells. In addition, knockdown of FGF13 reduced bevacizumab-induced glioma invasion.

FGFs are widely distributed in both normal cells and cancer cells, and have a wide range of biological activities including cell proliferation, differentiation, and migration. In glioblastoma, several FGFs are known to be involved in pathogenesis or malignancy (20). Generally, FGFs act through their specific signals by binding to their receptors. However, FGF13 (FHF2) and other FHF family members (FGF11, FGF12 and FGF14) lack a secretory portion (SP) and therefore, FGF13 cannot be secreted or bind to cell surface FGF receptors. FGF13 is involved in the intracellular regulatory mechanism. Wu et al. reported that FGF13 regulated tubulin dynamics and invasive activity in neurons (14). Recently, the role of FGF13 in several cancers was also investigated. Okada et al. investigated the overexpression of FGF13 in HeLa cisR cells, which caused greater resistance to cisplatin. Cervical cancer patients with higher FGF13-positive cells showed poor prognosis after chemoradiotherapy (21). Yu et al. reported high expression of FGF13 in the cytoplasm, which was associated with a shortened time to biochemical recurrence after surgery in

prostate cancer (22). Less has been reported on the role of FGF13 in glioma. Saito et al. reported that FGF13 was highly expressed in γ-secretase inhibitor non-responder group when compared with responder group (23). Other studies reported the knockdown of SOX2 changed FGF13 expression in glioblastoma (24) (25). However, the functional role of FGF13 in glioma was not fully elucidated. We found that cytoplasmic FGF13 regulated tubulin dynamics and glioma invasion.

Recently, a number of studies found the cytoskeleton had an important role in glioma invasion (15) (26). The cytoskeleton consists of three major classes of structural components, including the microtubules (tubulin), actin filaments (actin), and intermediate filaments. In particular, microtubules and actin filaments are important in cell motility, and the crosstalk between these proteins is also important in cell migration (27). Both protein types are found in the cytoplasm but can be distributed in different parts of the cytoplasm. Some tubulin-associated proteins have been reported to regulate glioma invasion. Dráberová et al. showed that silencing of the microtubules severing ATPase spastin in human glioblastoma cells inhibited cell motility (28). Song et al. demonstrated that silencing of the microtubule-destabilizing phosphoprotein, stathmin, inhibited invasion and increased chemosensitivity of cancer stem cells (29). Also, many tubulin targeted therapies have been reported and showed

clinical benefit in glioma, including the microtubule stabilizing tubulin-binding agent patupilone (30), valproic acid (31), and tumor-treating fields (TTFields) (32). We first reported that FGF13 regulated glioma invasion by stabilizing microtubules in the leading edge of the tumor, and that silencing of FGF13 *in vivo* significantly prolonged the survival time of xenograft models. However, as previously reported, the survival benefit achieved by inhibiting invasion has little impact (26). Three possible reasons could explain the survival benefit derived from FGF13 deletion. First, it is possible that inhibition of glioma invasion may prolong xenograft survival. Whether inhibition of glioma invasion could prolong survival is not well-known. Nagai, et al. reported that regulation of invasion did not change the survival time (33). In contrast, Hayashi, et al. showed that inhibition of glioma invasion could significantly prolong survival time, but the number of survival benefit days was within 15% of the OS time (26). Our xenograft models showed a survival benefit; however, the number of survival benefit days were 17.6%, 9.8%, and 14.7% in J3T-2, MGG8 and MGG23 cells, respectively. These percentage are agreement with those of Hayashi et al. Second, it is also possible that other cellular processes related to microtubules were dysfunctional and this led to tumor cell death. Microtubules are highly dynamic structures that play important roles in cells, including vesicular transport processes other than during mitosis or migration. Third,

it is possible that FGF13 interacts with voltage-gated sodium channel proteins (Na_Vs) in neurons (34) and may also interact with Na_Vs in some cancers (21) (22). Na_Vs is essential for glioma formation, so it may change the survival time in xenograft models.

Randomized, placebo-controlled phase III trials of AVAglio and RTOG-0825 in newly diagnosed glioblastoma, with the addition of bevacizumab to radiotherapy plus temozolomide, could not prolong OS (2) (3). One reason for this result could be that anti-VEGF therapy induced a phenotypic shift (35) toward a more invasive, aggressive, and treatment-resistant phenotype. Some signaling pathway such as MET (36), PI3K, or Wnt (37) are known to be activated to promote invasion after bevacizumab treatment. We showed that FGF13 was also involved in bevacizumab-induced glioma invasion in animal model. We thought FGF13 expression might be increased to induce invasion after bevacizumab treatment. But western blotting data of U87ΔEGFR cells and U251 cells indicated that the expression level of FGF13B were not changed after bevacizumab treatment. Microarray data for human specimens also showed same result, although we did not show FGF13A and FGF13B separately in this data. It is possible that FGF13B, which is mainly expressed in cytoplasm, is only increased in human specimens. These results may suggest that FGF13 is an innate factor which drives glioma invasion, and glioma cells remain dependent on FGF13

for their invasion after bevacizumab treatment. Delay et al. reported that patients in their secondary dataset with high expression of FGF13 before bevacizumab treatment showed shorter overall survival after bevacizumab treatment (19). Combination of some drugs like cilengitide (6) or altiratinib (38) with bevacizumab were previously reported to suppress bevacizumab-induced glioma invasion, therefore, FGF13 also could be a novel target of bevacizumab treatment.

In conclusion, our research first reported that FGF13 was mainly expressed in the cytoplasm of glioma cells and in the invasive edges of tumor specimens, and was therefore related to glioma invasion. Furthermore, FGF13 was also related to bevacizumab-induced glioma invasion. Our results suggested that FGF13 could be a promising new target to treat and prevent glioma invasion.

Materials and Methods

Culture of established cell lines and glioma stem cells

As previously reported, the canine glioma cell lines, J3T-1 and J3T-2, were derived from the same parental glioma cells (J3T) and were characterized (8, 39). The J3T cell line was a gift from Dr. Michael E. Berens at Barrow Neurological Institute (40). The A172, and Gli36Δ5 (41) cells were obtained from Dr. E. A. Chiocca at Massachusetts General Hospital, Boston, MA, USA. The U87ΔEGFR and U251 cells were obtained from Dr. Balveen Kaur at Ohio State University, Columbus, OH, USA. The human glioblastoma derived cancer stem cell line, MGG8 and MGG23 cells were provided by Dr. Hiroaki Wakimoto at Massachusetts General Hospital. NHA cells were purchased from Takara Bio Inc. (Shiga, Japan). The J3T-1, J3T-2, U87ΔEGFR, U251, LNZ308, A172, and Gli36Δ5 were cultured in Dulbecco's Modified Eagle's Medium (DMEM) containing 10% fetal bovine serum (FBS), 100 U of penicillin, and 0.1 mg mL^{-1} of streptomycin. The human glioblastoma derived cancer stem cell line, MGG8 and MGG23 cells were cultured as previously described (42) (18). For hypoxic conditions, the cells were cultured with 1% O_2 or in medium containing 100 μM deferoxamine mesylate (Sigma-Aldrich, St. Louis, MO, USA). U87 Δ EGFR, U251 and

A172 were authenticated by Promega (Madison, WI, USA) via short tandem repeat (STR) profiling in December 2016. Mycoplasma is negative in all cells.

Human glioblastoma specimens

Twenty-five human glioblastoma specimens were randomly selected from 80 glioblastoma patients treated at the Okayama University Hospital between 2006 and 2016. The study (1603-070) was approved by the ethical committee of the Okayama University Graduate School of Medicine, Dentistry and Pharmaceutical Sciences, Okayama, Japan. Informed consent was obtained from all patients included in the study. For pathological analyses, we defined the tumor core and the invasion edge as corresponding to the cellular tumor and infiltrating tumor as defined in the IVY Glioblastoma Atlas Project (http://glioblastoma.alleninstitute.org/). Among 25 specimens, all included the region of tumor core, but only 8 specimens had the region of invasion edge. We also evaluated FGF13 mRNA of 12 corresponding tumors from frozen samples that were available for qRT-PCR.

Microarray assays

Total RNA from J3T-1 and J3T-2 cells were isolated using the RNeasy kit (Qiagen, Santa

Clarita, CA, USA) and were analyzed using a GeneChip® Canine Genome 2.0 Array (Affymetrix, Santa Clara, CA, USA). The microarray analyses were performed by Takara Bio. Inc.. Briefly, biotinylated cRNA was synthesized by the GeneChip® 3'IVT Express Kit (Affymetrix) from 250 ng total RNA, according to the manufacturer's instructions. Biotinylated cRNA yields were checked with the NanoDrop ND-2000 Spectrophotometer (ThermoFisher Scientific, Scotts Valley, CA, USA). Following fragmentation, 10 μg of cRNA were hybridized for 16 hours at 45˚C on the GeneChip® Canine Genome 2.0 array. Arrays were washed and stained using the GeneChip® Fluidics Station 450 instrument (Affymetrix). Arrays were scanned using the GeneChip® Scanner 3000 7G (Affymetrix). Single array analyses were calculated using the Microarray Suite version 5.0 (MAS5.0) with Affymetrix default settings and global scaling as the normalization methods. The trimmed mean target intensity of each array was arbitrarily set to 500. Genes with absolute value of the fold change (FC) at least 2.0 and p-value < 0.05 were considered to be significantly regulated. GO enrichment analysis was performed using the functional annotation tool Database for Annotatio Visualization and Integrated Discovery (DAVID) 6.8 and significant GO terms were identified at $p < 0.05$ (43). All data are deposited in the Gene Expression Omnibus (accession number GSE88740).

RNA isolation, cDNA synthesis, and quantitative reverse transcription-polymerase chain reaction (qRT-PCR)

We isolated total RNA ─from the cell lines or human glioblastoma specimens, and synthesized cDNA with the SuperScript™ III First-Strand Synthesis System (Invitrogen, Carlsbad, CA, USA). The qRT-PCR reactions were then performed and detected using the StepOnePlus™ system (Life Technologies, Carlsbad, CA, USA).

As an internal control, we used β-actin (ACTB) mRNA. Primers were designed with the Primer3 Plus software and were purchased from Invitrogen. The primer sequences used were as follows:

Canine FGF13 primers: forward, 5′-GTAGCCAGTGAGGGCAAGAC-3′; reverse, 5′-AGTCTGCTGCACAAGCTCAA-3′.

Canine ACTB primers: forward, 5′-TGCGTGACATCAAGGAGAAG-3′; reverse, 5′-AGGAAGGAAGGCTGGAAGAG-3′.

Human FGF13 primers: forward, 5′-ACAAGCCTGCAGCTCATTTT-3′; reverse, 5′-CATTGTGGCTCATGGATTTG-3′.

Human CA9 primers: forward, 5’-TATCTGCACTCCTGCCCTCT-3’, 5’-

ACAGGACAGTTACCGGCTC-3'.

Human ACTB primers: forward, 5′-GGACTTCGAGCAAGAGATGG-3′; reverse, 5′-AGCACTGTGTTGGCGTACAG-3′.

Plasmids, RNA interference, and lentiviruses

The human FGF13B plasmids were purchased from GeneCopoeia (Rockville, MD, USA). We added a nuclear export signal to the N-terminus of FGF13B to avoid the nuclear import of overexpressed FGF13B, as previously reported (14). Small interfering RNA (siRNA) against canine or human FGF13 and negative control RNA were obtained from Thermo Fisher Scientific and transfected with Lipofectamine® 3000. The lentivirus encoding scramble short hairpin RNA (shRNA) and shRNA against canine or human FGF13 were prepared using the pLKO.1, psPAX2, and pMD2.G plasmids (Addgene, Cambridge, CA, USA), 293FT cells, and FuGENE® 6 Transfection Reagent (Promega) according to manufacturer's recommendations.

Migration and invasion assay

For scratch assays, we seeded each cells at 70–90% confluency. One day before the scratch,

we changed the medium into DMEM with 0.1% FBS for starvation. Then, the cells were scratched, cultured for 24 hours, and observed. The transwell and invasion assay were performed using a ThinCert^{TM} Tissue Culture Insert (Greiner Bio-One, Frickenhausen, Germany) and ~~a~~ BioCoat Matrigel invasion chamber (BD Bioscience, Franklin Lakes, NJ, USA) according to the manufacture's instructions, respectively. In brief, we seeded 1×10^5 cells in DMEM with 0.1% FBS in the upper chamber and filled with DMEM with 10% FBS in lower chamber. After 24 hours incubation, the filters of inserts were fixed with methanol and stained with Giemsa solution. We calculated the number of invading cells on the lower surface of the filter.

Western blot analysis

We prepared cell lysates and proteins using RIPA buffer and PMSF (Cell Signaling Technology), and isolated tubulin as previously described (14). And then, we performed western blotting as previously described (44).

After blocking, the membranes were incubated overnight with primary antibodies [anti-FGF13, Sigma-Aldrich, 1:300 dilution; anti-β-actin, Sigma-Aldrich, 1:5000 dilution; anti-acetylated-tubulin, Abcam, Cambridge, UK, 1:1000; anti-α-tubulin, Cell Signaling

Technology, Danvers, MA, USA, 1:1000] at 4°C. The secondary antibodies used were HRP-conjugated anti-mouse IgG and HRP-conjugated anti-rabbit IgG (Cell Signaling Technology, 1:5000). HRP signals were analyzed by the VersaDoc® molecular imaging system (Bio-Rad, Hercules, CA, USA).

Immunofluorescence and immunohistochemistry

Immunofluorescent and immunohistochemistry analyses were carried out as previously described (6) (11). Following antibodies were used for immunofluorescent: anti-FGF13, 1:100; anti-β-tubulin, Sigma-Aldrich, 1:1000; anti-vimentin, DakoCytomation, Carpentaria, CA, USA, 1:100; anti-ki67, Leica Biosystems, Wetzlar, Germany, 1:150; Alexa Fluor® 488- or Alexa Fluor® 594-conjugated antibodies, Life Technologies, 1:250. F-actin was stained using the CytoPainter F-actin Labeling Kit (Abcam) according to the manufacturer's protocol. Immunofluorescent images were obtained with a confocal laser microscope (LSM 780; Zeiss, Jena, Germany).

The following antibodies were used for immunohistochemistry: anti-FGF13, 1:100; anti-HLA, Abcam, 1:100; anti-CD31, Abcam, 1:50; anti-Iba-1, Abcam, 1:250; anti-goat IgG-HRP; Santa Cruz, 1:200. The Dako Envision®+ System-HRP Kit was then used in accordance

with the manufacturer's protocol (DakoCytomation) and the sections were counterstained with hematoxylin. Immunohistochemistry samples were observed with the BZ-8100 microscope (Keyence, Osaka, Japan).

Apoptosis assay

Apoptotic tumor cells were detected using an In Situ Cell Death Detection Kit (Roche, Mannheim, Germany) according to manufacture's protocol.

Water soluble tetrazolium-1 (WST-1) assay

For analyses of glioma cell proliferation, the WST-1 assay was performed according to the manufacturer's protocol (Roche).

In vivo experiments

All experimental animals were housed and handled in accordance with the guidelines of the Okayama University Animal Research Committee and all of the procedures and animal protocols were approved by the Committee on the Ethics of Animal Experimentation at Okayama University. Six week-old female athymic or SCID mice were purchased from Clea

Japan Inc. (Tokyo, Japan) or Charles River Laboratories Japan (Yokohama, Japan), respectively. The J3T-2, MGG8, MGG23, or U87ΔEGFR cells (2×10^5 cells) expressing scramble short hairpin RNA (shRNA) or shRNA against canine or human FGF13 were stereotaxically injected into the right frontal lobe (3 mm lateral to the midline, 1 mm anterior to the coronal suture, 3 mm depth from the dura), using a stereotactic frame (Narishige, Tokyo, Japan) and Hamilton syringe (Hamilton, Reno, NV, USA) as previously described (6). Mice bearing U87ΔEGFR cells were randomized into control or treatment groups. We administered PBS or bevacizumab (6 mg/kg) intraperitoneally three times per week, which we started on day 5 after implantation. Bevacizumab was provided by Chugai Pharmaceutical Co. (Tokyo, Japan). Group allocation was not blinded.

Statistical analyses

Statistical analyses were performed using SPSS statistical software (version 20; SPSS, Chicago, IL, USA). The results of percentages of FGF13 positive cells, the MIB-1 labeling indices, vessel density, percentages of TUNEL positive-cells and the relative mRNA and protein expression were analyzed using Student's *t*-tests. The results of relative mRNA expression, migration assays, WST-1 assays, percentages of TUNEL-positive cells and

invasion assays were analyzed using the two-way analysis of variance (ANOVA) test. Kaplan-Meier curves were compared using the log-rank test. *P* values of < 0.05 were considered statistically significant. For statistical analyses, experimental replicates from at least three samples were compiled for each experiment, unless otherwise stated in the figure legend. The data represent the mean ± SEM.

Supplementary Information accompanies the paper on the *Oncogene* website (http://www.nature.com/onc).

Conflict of interest

The authors have no conflicts of interest to declare. The authors have no personal, financial, or institutional interest in any of the drugs, materials, or devices described in this article.

Acknowledgements

This study was supported by grants-in-aid for Scientific Research from the Japanese Ministry of Education, Culture, Sports, Science, and Technology to T.I. (No. 22591611; No. 25462261) and K.K. (No. 23592125; No. 26462182). We thank Dr. H. Wakimoto at Massachusetts General Hospital for providing the human glioblastoma derived cancer stem

cell line (42) (18). We thank M. Arao and U. Ukai in the Department of Neurological Surgery and A. Ueda in the Department of Physiology for their technical assistance. The following medical students also contributed to our experiments: K. Yamamoto and Y. Inoue.

References

1. Stupp R, Mason WP, van den Bent MJ, Weller M, Fisher B, Taphoorn MJ, et al. Radiotherapy plus concomitant and adjuvant temozolomide for glioblastoma. N Engl J Med. 2005;352(10):987-96.

2. Chinot OL, Wick W, Mason W, Henriksson R, Saran F, Nishikawa R, et al. Bevacizumab plus radiotherapy-temozolomide for newly diagnosed glioblastoma. N Engl J Med. 2014;370(8):709-22.

3. Gilbert MR, Dignam JJ, Armstrong TS, Wefel JS, Blumenthal DT, Vogelbaum MA, et al. A randomized trial of bevacizumab for newly diagnosed glioblastoma. N Engl J Med. 2014;370(8):699-708.

4. Piao Y, Liang J, Holmes L, Zurita AJ, Henry V, Heymach JV, et al. Glioblastoma resistance to anti-VEGF therapy is associated with myeloid cell infiltration, stem cell accumulation, and a mesenchymal phenotype. Neuro Oncol. 2012;14(11):1379-92.

5. Onishi M, Ichikawa T, Kurozumi K, Fujii K, Yoshida K, Inoue S, et al. Bimodal anti-glioma mechanisms of cilengitide demonstrated by novel invasive glioma models. Neuropathology. 2013;33(2):162-74.

6. Ishida J, Onishi M, Kurozumi K, Ichikawa T, Fujii K, Shimazu Y, et al. Integrin

inhibitor suppresses bevacizumab-induced glioma invasion. Transl Oncol. 2014;7(2):292-302.e1.

7. Scherer HJ. A CRITICAL REVIEW: THE PATHOLOGY OF CEREBRAL GLIOMAS. J Neurol Psychiatry. 1940;3(2):147-77.

8. Inoue S, Ichikawa T, Kurozumi K, Maruo T, Onishi M, Yoshida K, et al. Novel animal glioma models that separately exhibit two different invasive and angiogenic phenotypes of human glioblastomas. World Neurosurg. 2012;78(6):670-82.

9. Maruo T, Ichikawa T, Kanzaki H, Inoue S, Kurozumi K, Onishi M, et al. Proteomics-based analysis of invasion-related proteins in malignant gliomas. Neuropathology. 2013;33(3):264-75.

10. Onishi M, Ichikawa T, Kurozumi K, Date I. Angiogenesis and invasion in glioma. Brain Tumor Pathol. 2011;28(1):13-24.

11. Onishi M, Ichikawa T, Kurozumi K, Inoue S, Maruo T, Otani Y, et al. Annexin A2 regulates angiogenesis and invasion phenotypes of malignant glioma. Brain Tumor Pathol. 2015;32(3):184-94.

12. Smallwood PM, Munoz-Sanjuan I, Tong P, Macke JP, Hendry SH, Gilbert DJ, et al. Fibroblast growth factor (FGF) homologous factors: new members of the FGF family

implicated in nervous system development. Proc Natl Acad Sci U S A. 1996;93(18):9850-7.

13. Nishimoto S, Nishida E. Fibroblast growth factor 13 is essential for neural differentiation in Xenopus early embryonic development. J Biol Chem. 2007;282(33):24255-61.

14. Wu QF, Yang L, Li S, Wang Q, Yuan XB, Gao X, et al. Fibroblast growth factor 13 is a microtubule-stabilizing protein regulating neuronal polarization and migration. Cell. 2012;149(7):1549-64.

15. Fujimura A, Michiue H, Cheng Y, Uneda A, Tani Y, Nishiki T, et al. Cyclin G2 promotes hypoxia-driven local invasion of glioblastoma by orchestrating cytoskeletal dynamics. Neoplasia. 2013;15(11):1272-81.

16. Berges R, Balzeau J, Peterson AC, Eyer J. A tubulin binding peptide targets glioma cells disrupting their microtubules, blocking migration, and inducing apoptosis. Mol Ther. 2012;20(7):1367-77.

17. Katsetos CD, Reginato MJ, Baas PW, D'Agostino L, Legido A, Tuszyn Ski JA, et al. Emerging microtubule targets in glioma therapy. Semin Pediatr Neurol. 2015;22(1):49-72.

18. Wakimoto H, Mohapatra G, Kanai R, Curry WT, Jr., Yip S, Nitta M, et al. Maintenance of primary tumor phenotype and genotype in glioblastoma stem cells. Neuro

Oncol. 2012;14(2):132-44.

19. DeLay M, Jahangiri A, Carbonell WS, Hu YL, Tsao S, Tom MW, et al. Microarray analysis verifies two distinct phenotypes of glioblastomas resistant to antiangiogenic therapy. Clin Cancer Res. 2012;18(10):2930-42.

20. Wang F, Yang L, Shi L, Li Q, Zhang G, Wu J, et al. Nuclear translocation of fibroblast growth factor-2 (FGF2) is regulated by Karyopherin-beta2 and Ran GTPase in human glioblastoma cells. Oncotarget. 2015;6(25):21468-78.

21. Okada T, Murata K, Hirose R, Matsuda C, Komatsu T, Ikekita M, et al. Upregulated expression of FGF13/FHF2 mediates resistance to platinum drugs in cervical cancer cells. Sci Rep. 2013;3:2899.

22. Yu L, Toriseva M, Tuomala M, Seikkula H, Elo T, Tuomela J, et al. Increased expression of fibroblast growth factor 13 in prostate cancer is associated with shortened time to biochemical recurrence after radical prostatectomy. Int J Cancer. 2016;139(1):140-52.

23. Saito N, Fu J, Zheng S, Yao J, Wang S, Liu DD, et al. A high Notch pathway activation predicts response to gamma secretase inhibitors in proneural subtype of glioma tumor-initiating cells. Stem Cells. 2014;32(1):301-12.

24. Fang X, Yoon JG, Li L, Yu W, Shao J, Hua D, et al. The SOX2 response program in

glioblastoma multiforme: an integrated ChIP-seq, expression microarray, and microRNA analysis. BMC Genomics. 2011;12:11.

25. Berezovsky AD, Poisson LM, Cherba D, Webb CP, Transou AD, Lemke NW, et al. Sox2 promotes malignancy in glioblastoma by regulating plasticity and astrocytic differentiation. Neoplasia. 2014;16(3):193-206, .e19-25.

26. Hayashi K, Michiue H, Yamada H, Takata K, Nakayama H, Wei FY, et al. Fluvoxamine, an anti-depressant, inhibits human glioblastoma invasion by disrupting actin polymerization. Sci Rep. 2016;6:23372.

27. Fife CM, McCarroll JA, Kavallaris M. Movers and shakers: cell cytoskeleton in cancer metastasis. Br J Pharmacol. 2014;171(24):5507-23.

28. Draberova E, Vinopal S, Morfini G, Liu PS, Sladkova V, Sulimenko T, et al. Microtubule-severing ATPase spastin in glioblastoma: increased expression in human glioblastoma cell lines and inverse roles in cell motility and proliferation. J Neuropathol Exp Neurol. 2011;70(9):811-26.

29. Song Y, Mu L, Han X, Liu X, Fu S. siRNA targeting stathmin inhibits invasion and enhances chemotherapy sensitivity of stem cells derived from glioma cell lines. Acta Biochim Biophys Sin (Shanghai). 2014;46(12):1034-40.

30. Oehler C, Frei K, Rushing EJ, McSheehy PM, Weber D, Allegrini PR, et al. Patupilone (epothilone B) for recurrent glioblastoma: clinical outcome and translational analysis of a single-institution phase I/II trial. Oncology. 2012;83(1):1-9.

31. Barker CA, Bishop AJ, Chang M, Beal K, Chan TA. Valproic acid use during radiation therapy for glioblastoma associated with improved survival. Int J Radiat Oncol Biol Phys. 2013;86(3):504-9.

32. Stupp R, Taillibert S, Kanner AA, Kesari S, Steinberg DM, Toms SA, et al. Maintenance Therapy With Tumor-Treating Fields Plus Temozolomide vs Temozolomide Alone for Glioblastoma: A Randomized Clinical Trial. JAMA. 2015;314(23):2535-43.

33. Nagai S, Moreno O, Smith CA, Ivanchuk S, Romagnuolo R, Golbourn B, et al. Role of the cofilin activity cycle in astrocytoma migration and invasion. Genes Cancer. 2011;2(9):859-69.

34. Wittmack EK, Rush AM, Craner MJ, Goldfarb M, Waxman SG, Dib-Hajj SD. Fibroblast growth factor homologous factor 2B: association with Nav1.6 and selective colocalization at nodes of Ranvier of dorsal root axons. J Neurosci. 2004;24(30):6765-75.

35. Ichikawa T, Otani Y, Kurozumi K, Date I. Phenotypic Transition as a Survival Strategy of Glioma. Neurol Med Chir (Tokyo). 2016;56(7):387-95.

36. Lu KV, Chang JP, Parachoniak CA, Pandika MM, Aghi MK, Meyronet D, et al. VEGF inhibits tumor cell invasion and mesenchymal transition through a MET/VEGFR2 complex. Cancer Cell. 2012;22(1):21-35.

37. Keunen O, Johansson M, Oudin A, Sanzey M, Rahim SA, Fack F, et al. Anti-VEGF treatment reduces blood supply and increases tumor cell invasion in glioblastoma. Proc Natl Acad Sci U S A. 2011;108(9):3749-54.

38. Piao Y, Park SY, Henry V, Smith BD, Tiao N, Flynn DL, et al. Novel MET/TIE2/VEGFR2 inhibitor altiratinib inhibits tumor growth and invasiveness in bevacizumab-resistant glioblastoma mouse models. Neuro Oncol. 2016;18(9):1230-41.

39. Hampl JA, Camp SM, Mydlarz WK, Hampl M, Ichikawa T, Chiocca EA, et al. Potentiated gene delivery to tumors using herpes simplex virus/Epstein-Barr virus/RV tribrid amplicon vectors. Hum Gene Ther. 2003;14(7):611-26.

40. Berens ME, Bjotvedt G, Levesque DC, Rief MD, Shapiro JR, Coons SW. Tumorigenic, invasive, karyotypic, and immunocytochemical characteristics of clonal cell lines derived from a spontaneous canine anaplastic astrocytoma. In Vitro Cell Dev Biol Anim. 1993;29a(4):310-8.

41. Ichikawa T, Hogemann D, Saeki Y, Tyminski E, Terada K, Weissleder R, et al. MRI

of transgene expression: correlation to therapeutic gene expression. Neoplasia. 2002;4(6):523-30.

42. Wakimoto H, Kesari S, Farrell CJ, Curry WT, Jr., Zaupa C, Aghi M, et al. Human glioblastoma-derived cancer stem cells: establishment of invasive glioma models and treatment with oncolytic herpes simplex virus vectors. Cancer Res. 2009;69(8):3472-81.

43. Huang da W, Sherman BT, Lempicki RA. Systematic and integrative analysis of large gene lists using DAVID bioinformatics resources. Nat Protoc. 2009;4(1):44-57.

44. Oka T, Kurozumi K, Shimazu Y, Ichikawa T, Ishida J, Otani Y, et al. A super gene expression system enhances the anti-glioma effects of adenovirus-mediated REIC/Dkk-3 gene therapy. Sci Rep. 2016;6:33319.

Figure legends

Fig. 1

Distribution pattern of fibroblast growth factor 13 (FGF13) in glioma cell lines and human glioma specimens.

(A) Immunofluorescent staining of J3T-2 cells showed FGF13 was more dominant in the cytoplasm than nucleus. DAPI = 4, 6-diamidino-2-phenylindole, used for nuclear staining.

(B) Immunohistochemical staining of FGF13 in normal human brains showed FGF13 was mainly expressed in the nucleus of the neuron.

(C, D) The expression pattern of FGF13 in the tumor core and the invasion edge of 25 glioblastoma patients were evaluated using immunohistochemistry (IHC). Quantification was performed in randomly-selected three fields in each region. The representative results from cases 18 and 20 are shown in (C). The expression level of FGF13 mRNA determined from quantitative reverse transcription-polymerase chain reaction (qRT-PCR) was compared to the immunohistochemical staining of FGF13 from 12 corresponding tumors. The median expression values for FGF13 mRNA with upper and lower quartiles (25–75%) are shown and the expression levels of FGF13 mRNA and proteins were significantly correlated. The

correlations were determined using the Student's independent *t*-test.

(E) Western blotting confirmed FGF13B was more predominant than FGF13A. Representative western blots from three experiments are shown. Numerical values on the right side of panel represent quantification of the relative protein level by densitometry. Molecular weight markers are shown in parentheses.

(F) At the invasive edge, most tumor cells expressed FGF13 in the cytoplasm (n = 8). However, in the tumor core, the number of FGF13 positive cells varied in each patient (n = 25). The statistical significance was calculated by the Student's *t*-test.$^{*}p < 0.01$.

(G) Data of IVY Glioblastoma Atlas Project also showed that FGF13 was more expressed in the area of both leading edge and infiltrating tumor than cellular tumor, perinecrotic zone, hyperplastic blood vessels and microvascular proliferations.

(H) Data from the Cancer Genome Atlas (TCGA) project showed that FGF13 was more expressed in proneural and neural subtypes than in classical and mesenchymal subtypes.

Scale bars, 50 μm (A–C).

Fig. 2

FGF13 was involved in glioma migration *in vitro*.

(A) Relative expression levels of FGF13 mRNA were decreased by siRNA in J3T-2, U87ΔEGFR, U251, and LNZ308 cells (n = 3).

(B) Knockdown of FGF13 by siRNA decreased both FGF13A and FGF13B protein levels in U87ΔEGFR, U251, and LNZ308 cells.

(C, D) Knockdown of FGF13 by siRNA decreased the migratory activity of J3T-2 (n = 10), U87ΔEGFR (n = 10), U251 (n = 10), and LNZ308 cells (n=5).

(E) Knockdown of FGF13 by siRNA did not affect the cell viability of J3T-2, U87ΔEGFR, U251, and LNZ308 cells (n = 5). Each cell sample was transfected with siRNA, and 48 hours later cell viability was calculated using the WST-1 assay.

Data are shown (A, D and E) as the mean ± SEM. Statistical significance was calculated by ANOVA with Dunnett's post hoc test. $^{*}p < 0.05$

NC = negative control siRNA.

Fig. 3

FGF13 was involved in glioma invasion in the J3T-2 xenograft model and reduction of FGF13 improved overall survival.

(A) The relative expression levels of FGF13 mRNA were decreased by shRNA in J3T-2 cells

(n = 3).

(B, C) Immunohistochemical staining [tumor cells: vimentin, red; nuclei: DAPI (4′, 6-diamino-2-phenylindole), blue] showed that the tumor border of samples from the J3T-2 cells transfected with lentivirus encoding FGF13 shRNA (J3T-2 FGF13 shRNA) was clear. The cell density in the tumor border was significantly less in the J3T-2 FGF13 shRNA samples. Scale bars, 100 μm.

(D, E) Knockdown of FGF13 by shRNA did not change the MIB-1 labeling index (n = 4).

(F, G and H) Knockdown of FGF13 did not induce cell apoptosis and increase the number of vessels (n=4)

(I) Kaplan-Meier survival curves of intracranial xenografts with J3T-2 expressing FGF13 shRNA or scramble shRNA. The survival percentage with time of the J3T-2 expressing FGF13 shRNA samples was significantly longer than that of the J3T-2 scrambles with shRNA (median survival = 59.5 versus 49 days, respectively) (n = 8). Statistical significance was calculated by the log rank test.

Data are shown (A, C, E, F, and H) as the mean ± SEM. Statistical significance was calculated by the Student's *t*-test. $^{*}p < 0.05$.

Fig. 4

FGF13 was involved in glioma invasion in the human glioblastoma-derived cancer stem cell xenograft model and reduction of FGF13 improved overall survival.

(A) The relative expression level of FGF13 mRNA was decreased by shRNA in MGG8 cells (n = 3).

(B, C) Immunohistochemical staining of representative sections of the intracranial xenograft with MGG8 cells expressing FGF13 shRNA or scramble shRNA. Tumor cells were stained with anti-human HLA antibody and the number of tumor cells in the ipsilateral and contralateral cortex was assessed (n = 4). Invasiveness was impaired in MGG8 cells transfected with lentivirus encoding FGF13 shRNA. Scale bars, 50 μm.

(D) Knockdown of FGF13 did not induce cell apoptosis (n=4).

(E) Kaplan-Meier survival curves of intracranial xenografts with MGG8 cells expressing FGF13 shRNA#1, FGF13 shRNA#2, or scramble shRNA. The survival time of MGG8 samples expressing either FGF13 shRNA#1 or FGF13 shRNA#2 (median survival = 61 or 61.5 days, respectively) were significantly longer than that of the MGG8 scramble shRNA expressing samples (median survival = 55.5 days) (n = 8). Statistical significance was calculated by the log rank test. $^{**}p < 0.02$.

Data are shown (A, C and D) as the mean ± SEM. Statistical significance was calculated by ANOVA with the Dunnett's post hoc test. $^{*}p < 0.01$.

Fig. 5

FGF13 colocalized with tubulin in the cytoplasm, stabilized tubulin and the FGF13 expression in glioma was negatively regulated by hypoxic condition.

(A) Immunohistochemical staining (FGF13, green; β-tubulin, red; F-actin, blue) of J3T-2 cells showed that cytoplasmic FGF13 was colocalized with tubulin.

(B) FGF13 stabilized and protected microtubules from nocodazole-induced tubulin depolymerization. Total, soluble and insoluble tubulins were prepared from normal A172 cells or A172 cells overexpressing FGF13B after treatment with DMSO or nocodazole (5μM, in DMSO) for 15 minutes at 37℃. DMSO = dimethyl sulfoxide; Ace-tubulin = acetylated tubulin; Tyr-tubulin = tyrosinated tubulin. Numerical values under the panel represent quantification of the relative protein level (Ace-tubulin / Tyr-tubulin) as assessed by densitometry.

(C) The expression levels of FGF13 in both U87 Δ EGFR and U251 cell lines were decrease by hypoxia or deferoxamine mesylate (DFOM, 100 μM).

Fig. 6

Knockdown of FGF13 inhibited bevacizumab-induced glioma invasion.

(A) The expression level of FGF13 in the U87 Δ EGFR was almost the same after bevacizumab treatment.

(B, C) The expression level of FGF13 mRNA in five glioblastoma patients at either pre- or post-bevacizumab treatment. There was no significant difference on FGF13 mRNA expression level between pre- and post-bevacizumab treatment. Bev = bevacizumab.

(D) The relative expression level of FGF13 mRNA was decreased by shRNA in U87ΔEGFR cells (n = 3). $^{*}p < 0.01$.

(E, F) Immunohistochemical staining of untreated U87ΔEGFR orthotopic tumors showed the expansion of the tumor with well-defined borders (E, left upper panel). After treatment with bevacizumab, the tumor border became irregular with tumor invasion (E, right upper panel). The invasiveness after bevacizumab treatment was assessed using the distance between the tumor mass edge and invasive lesion (F). The invasiveness was remarkably decreased in the U87ΔEGFR cells transfected with lentivirus encoding FGF13 shRNA (n = 4) compared with that of the U87ΔEGFR cells transfected with lentivirus encoding scramble shRNA (n = 5).

Data are shown as the mean ± SEM. Statistical significance was calculated by the Student's *t*-test. $^{*}p < 0.01$. $^{**}p < 0.05$. Scale bars, 200 μm (E).

Table 1. GO analysis of significantly up-regulated genes in J3T-1

GO term	Process description	P value	Fold enrichment
0005925	Focal adhesion	3.4E-9	4.2
0070062	Extracellular exosome	2.6E-5	1.6
0005887	Integral component of plasma membrane	3.8E-3	1.8
0005615	Extracellular space	4.3E-3	1.7
0009897	External side of plasma membrane	2.0E-2	2.7
0005623	Cytosol	4.4E-2	1.5
0030173	Integral component of Golgi membrane	4.6E-2	4.9

Table 2. GO analysis of significantly up-regulated genes in J3T-2

GO term	Process description	P value	Fold enrichment
0070062	Extracellular exosome	1.0E-7	1.8
0005911	Cell-cell junction	2.5E-3	3.8
0000790	Nuclear chromatin	5.8E-3	3.0
0030027	Lamellipodium	8.0E-3	3.5
0005615	Extracellular space	9.0E-3	1.6
0005768	Endosome	1.1E-2	3.0
0005874	microtubule	1.1E-2	3.3
0001725	Stress fiber	1.5E-2	5.2
0043234	Protein complex	2.3E-2	2.6
0005737	Cytoplasm	2.5E-2	1.3
0005856	Cytoskeleton	2.7E-2	3.0
0030864	Cortical actin cytoskeleton	3.2E-2	5.7
0030424	Axon	3.2E-2	2.9
0005578	Proteinaceous extracellular matrix	3.6E-2	2.4
0005925	Focal adhesion	4.3E-2	1.9
0005654	Nucleoplasm	4.4E-2	1.4
0005584	Collagen type I trimer	4.6E-2	42.7

Supplementary Table 1. Silencing of FGF13 did not alter perimeter of tumor cells

Name of cell lines	siRNA N.C.	siRNA #1	siRNA #2	Statistical significance (Compared with N.C.)
J3T2	191.5 1±14.8	177.0±11.5	177.9±13.4	N.S.
U87ΔEGFR	103.4±11.8	85.0±11.3	98.7±9.4	N.S.
U251	197.6±16.7	171.0±15.7	160.8±9.6	N.S.
LNZ308	137.2±6.3	129.0±6.5	128.1±7.1	N.S.
A172	212.5±14.5	202.9±24.9	199.0±15.6	N.S.
Gli36Δ5	136.1±10.2	162.0±13.8	157.2±14.3	N.S.

Data are shown as the mean ± SEM (μm). Statistical significance was calculated by ANOVA with Dunnett's post hoc test.
N.C. = negative control; N.S. = Not Significance

Supplementary Table 2. Silencing of FGF13 did not alter area of tumor cells

Name of cell lines	siRNA N.C.	siRNA #1	siRNA #2	Statistical significance (Compared with N.C.)
J3T2	388.4±16.2	402.0±42.2	413.4±14.3	N.S.
U87ΔEGFR	187.2±17.1	218.6±24.5	220.3±21.1	N.S.
U251	772.0±80.7	918.1±83,2	847.0±86.9	N.S.
LNZ308	972.1±75.1	848.1±96.8	869.6±69.9	N.S.
A172	479.3±41.0	549.6±42.4	523.7±49.4	N.S.
Gli36Δ5	866.2±75.2	720.0±69.3	888.2±90.7	N.S.

Data are shown as the mean ± SEM (μm^2). Statistical significance was calculated by ANOVA with Dunnett's post hoc test.
N.C. = negative control; N.S. = Not Significance

Figure 1

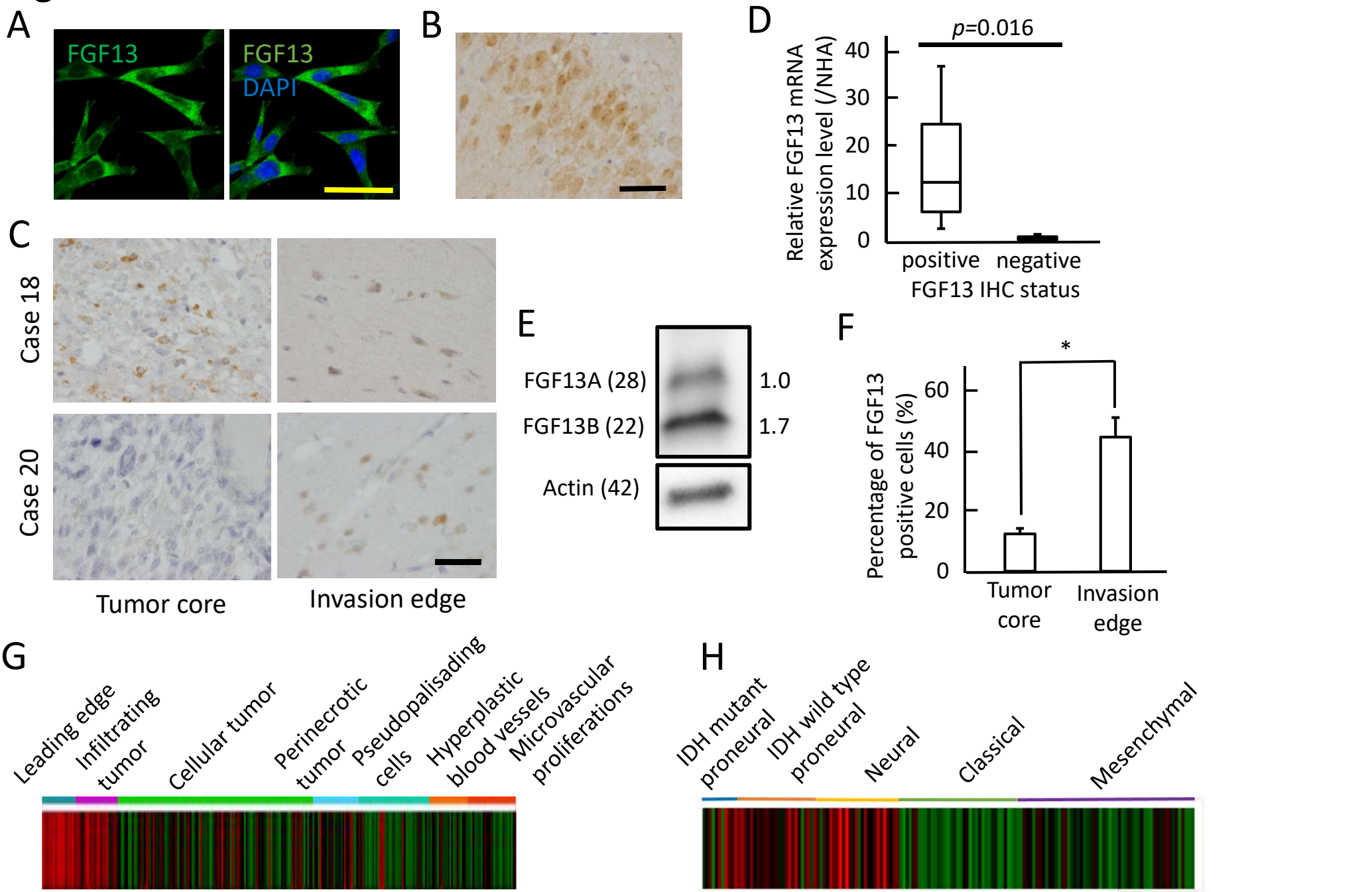
A
FGF13
FGF13
DAPI
B
C
Case 18
Case 20
Tumor core
Invasion edge
D
p=0.016
Relative FGF13 mRNA expression level (/NHA)
40
30
20
10
0
positive
negative
FGF13 IHC status
E
FGF13A (28)
FGF13B (22)
Actin (42)
1.0
1.7
F
*
Percentage of FGF13 positive cells (%)
60
40
20
0
Tumor core
Invasion edge
G
Leading edge
Infiltrating tumor
Cellular tumor
Perinecrotic tumor
Pseudopalisading cells
Hyperplastic blood vessels
Microvascular proliferations
H
IDH mutant proneural
IDH wild type proneural
Neural
Classical
Mesenchymal

Figure 2

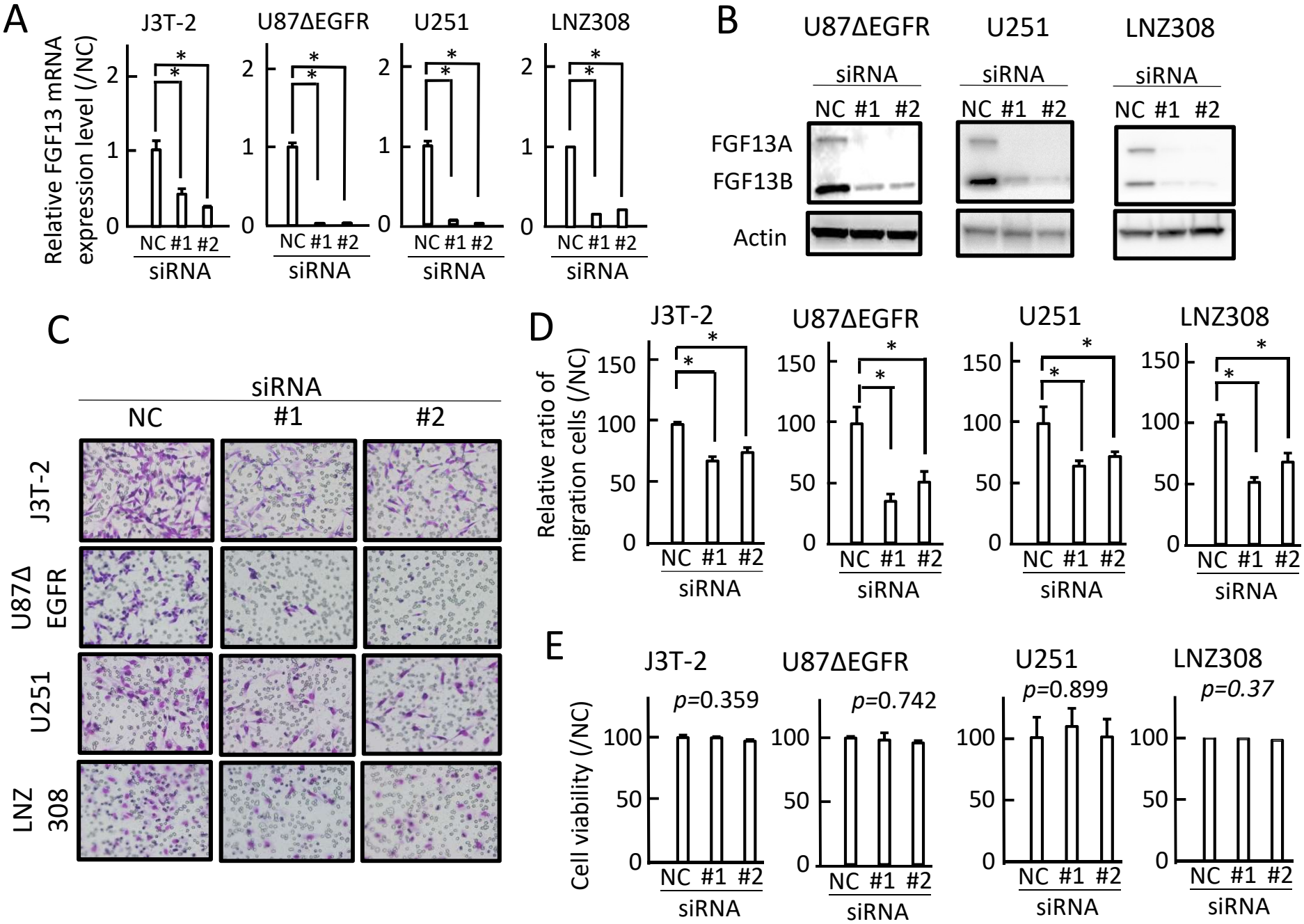
A
J3T-2
U87ΔEGFR
U251
LNZ308
Relative FGF13 mRNA expression level (/NC)
NC #1 #2
siRNA
B
U87ΔEGFR
U251
LNZ308
siRNA
NC #1 #2
FGF13A
FGF13B
Actin
C
siRNA
NC
#1
#2
J3T-2
U87Δ EGFR
U251
LNZ 308
D
Relative ratio of migration cells (/NC)
E
Cell viability (/NC)
p=0.359
p=0.742
p=0.899
p=0.37

Figure 3

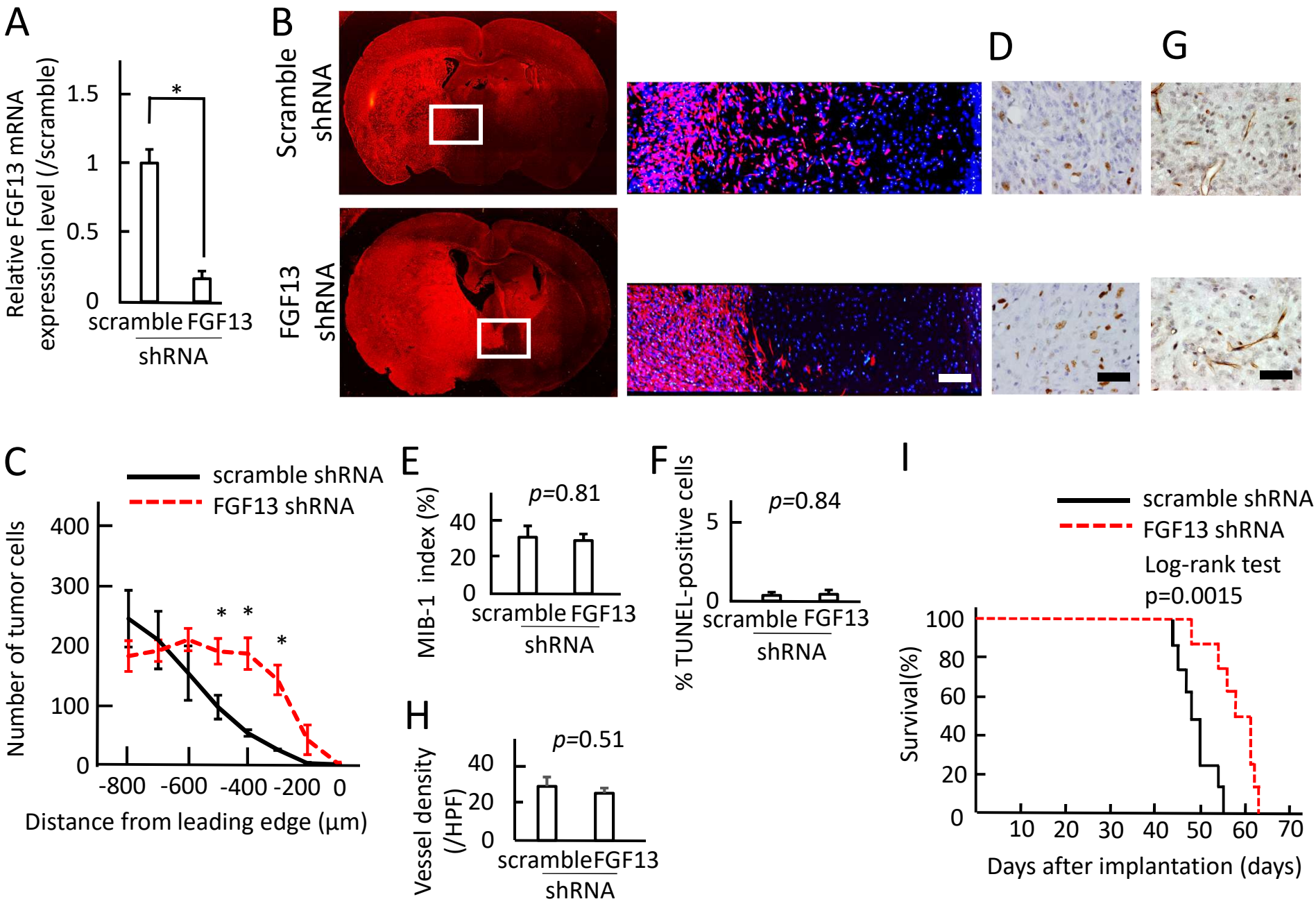
A
Relative FGF13 mRNA expression level (/scramble)
1.5
1
0.5
0
*
scramble
FGF13 shRNA
B
Scramble shRNA
FGF13 shRNA
D
G
C
scramble shRNA
FGF13 shRNA
Number of tumor cells
400
300
200
100
0
* * *
-800 -600 -400 -200 0
Distance from leading edge (μm)
E
MIB-1 index (%)
p=0.81
40
20
0
scramble FGF13 shRNA
F
% TUNEL-positive cells
p=0.84
5
0
scramble FGF13 shRNA
H
Vessel density (/HPF)
p=0.51
40
20
0
scrambleFGF13 shRNA
I
scramble shRNA
FGF13 shRNA
Log-rank test
p=0.0015
Survival(%)
100
80
60
40
20
0
10 20 30 40 50 60 70
Days after implantation (days)

Figure 4

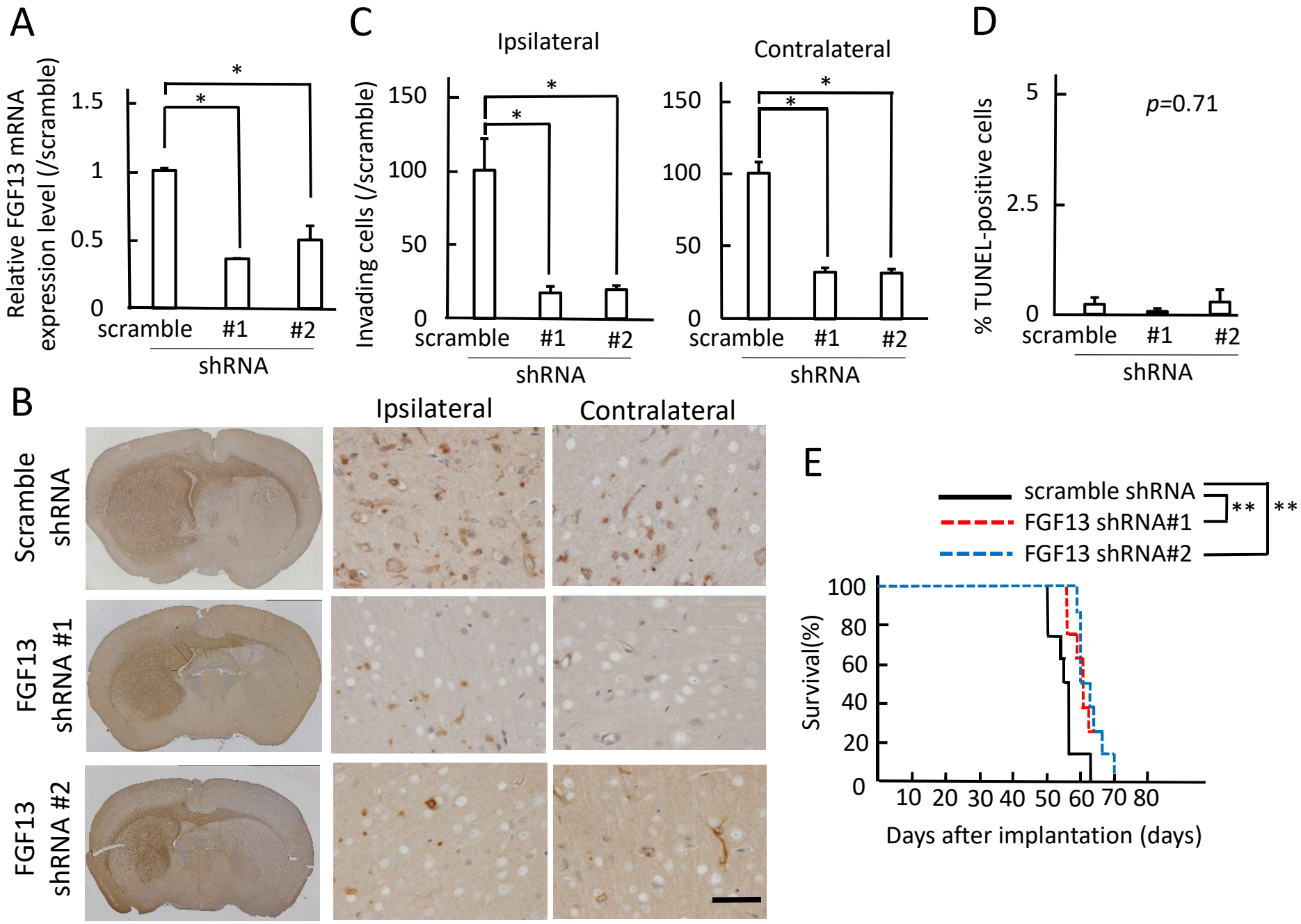
A
Relative FGF13 mRNA expression level (/scramble)
1.5
1
0.5
0
*
*
scramble
#1
#2
shRNA
C
Ipsilateral
Contralateral
Invading cells (/scramble)
150
100
50
0
*
*
scramble
#1
#2
shRNA
D
% TUNEL-positive cells
5
2.5
0
p=0.71
scramble
#1
#2
shRNA
B
Ipsilateral
Contralateral
Scramble shRNA
FGF13 shRNA #1
FGF13 shRNA #2
E
scramble shRNA
FGF13 shRNA#1
FGF13 shRNA#2
**
**
Survival(%)
100
80
60
40
20
0
10 20 30 40 50 60 70 80
Days after implantation (days)

Figure 5

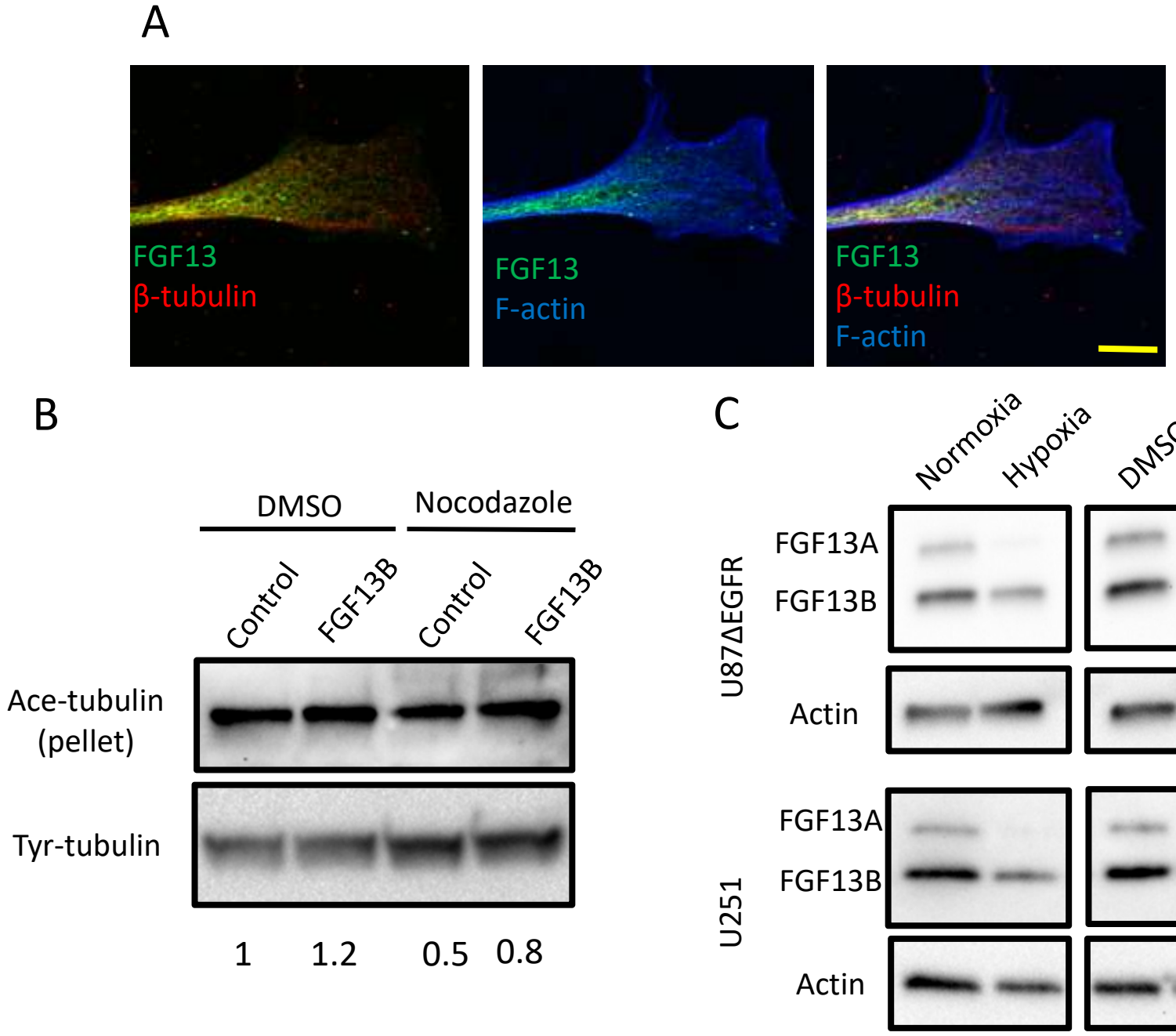
A
FGF13
β-tubulin
FGF13
F-actin
FGF13
β-tubulin
F-actin
B
DMSO
Nocodazole
Control
FGF13B
Control
FGF13B
Ace-tubulin
(pellet)
Tyr-tubulin
1
1.2
0.5
0.8
C
Normoxia
Hypoxia
DMSO
DFOM
U87ΔEGFR
FGF13A
FGF13B
Actin
U251
FGF13A
FGF13B
Actin

Figure 6

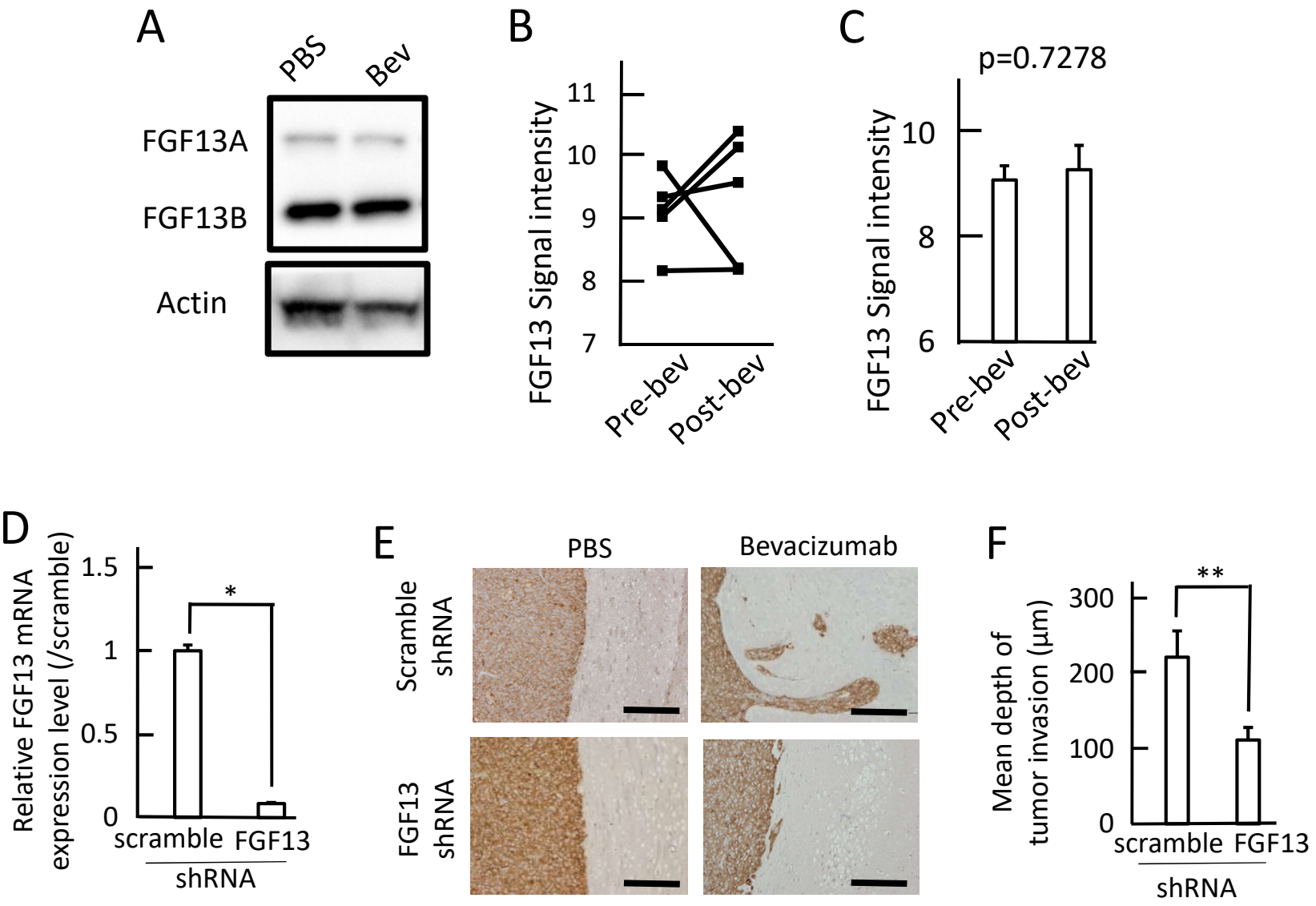
A
PBS
Bev
FGF13A
FGF13B
Actin
B
FGF13 Signal intensity
11
10
9
8
7
Pre-bev
Post-bev
C
p=0.7278
FGF13 Signal intensity
10
8
6
Pre-bev
Post-bev
D
Relative FGF13 mRNA expression level (/scramble)
1.5
1
0.5
0
*
scramble
FGF13
shRNA
E
PBS
Bevacizumab
Scramble shRNA
FGF13 shRNA
F
Mean depth of tumor invasion (μm)
300
200
100
0
**
scramble
FGF13
shRNA

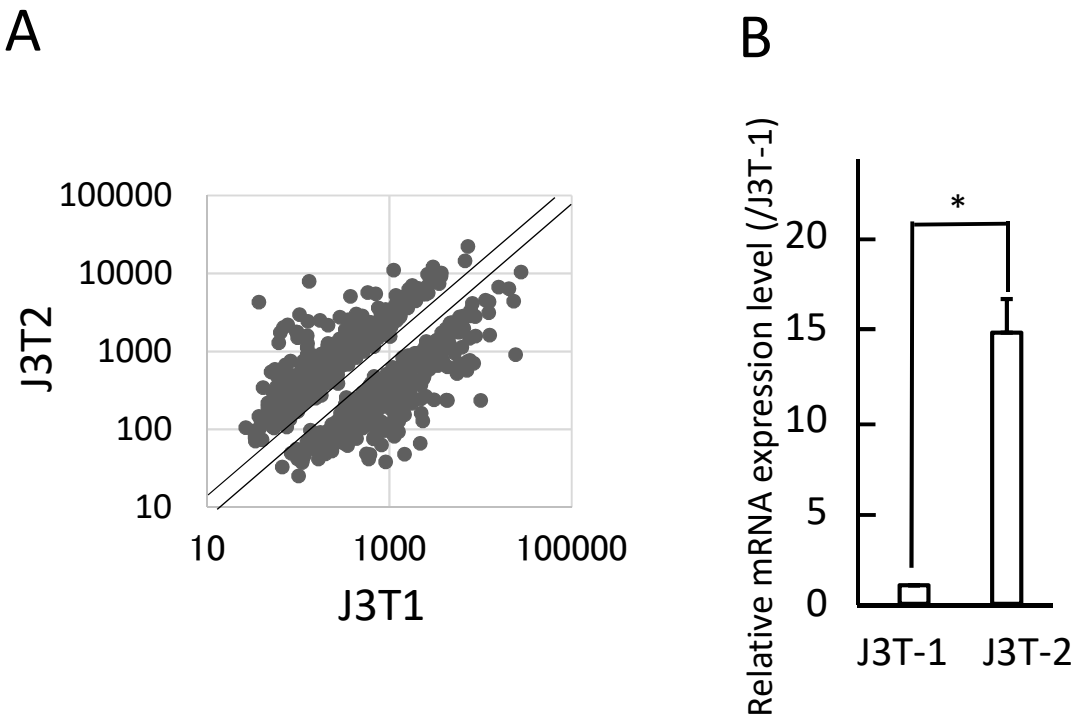

Supplementary Fig. 1

Microarray analysis of J3T-2 compared with J3T-1 identified novel invasion-related gene, FGF13.

(A) Microarray analysis showed 791 differentially expressed genes that presenting fold changes > 2.0 between J3T-1 and J3T-2, which consisted of 418 genes overexpressed in J3T-1 and 373 genes overexpressed in J3T-2.

(B) FGF13 mRNA expression was markedly up-regulated in J3T-2 than J3T-1 (n=6). Statistical significance was calculated by the Student's T-test. *$p < 0.01$.

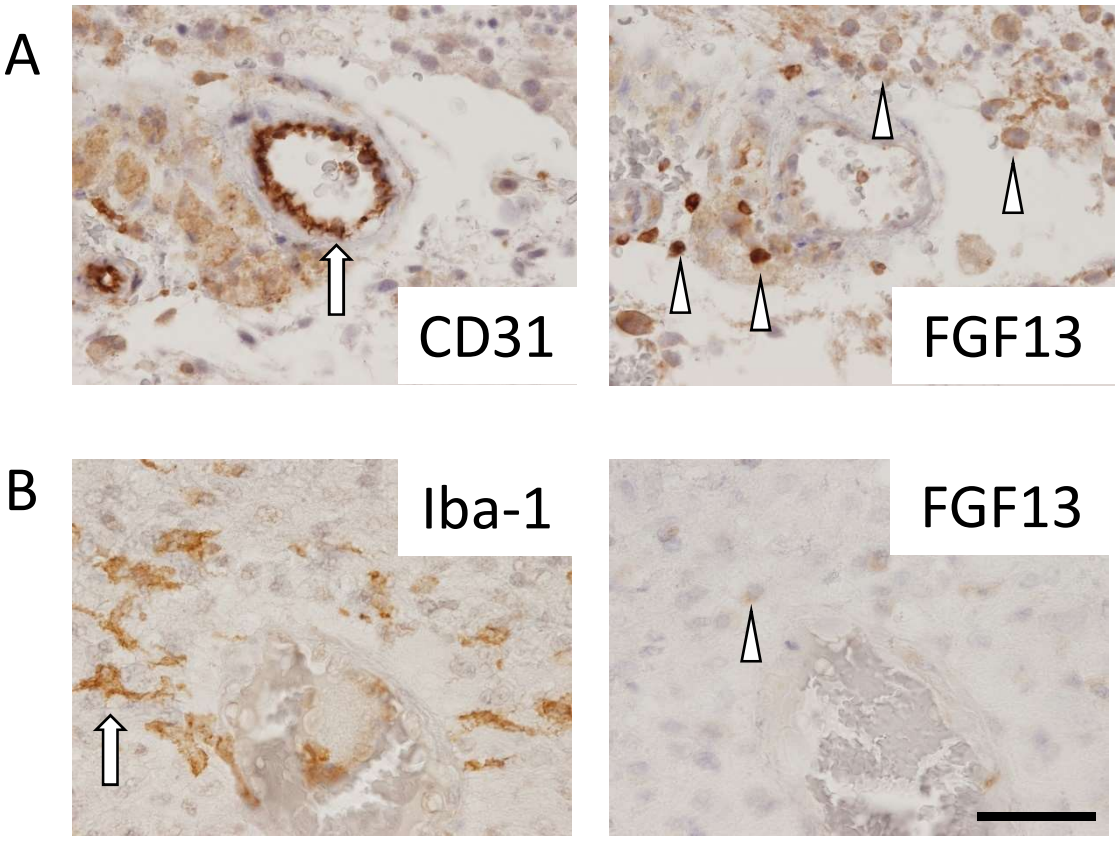

Supplementary Fig. 2
Microenvironmental cells like endothelial cells or macrophages did not express FGF13.
Serial section analysis in immunohistochemistry revealed that tumor cells expressed FGF13 (arrow head), however, endothelial cells (arrow, Fig. A) or macrophages (arrow, Fig. B) did not express FGF13.
Scale bar, 50 µm

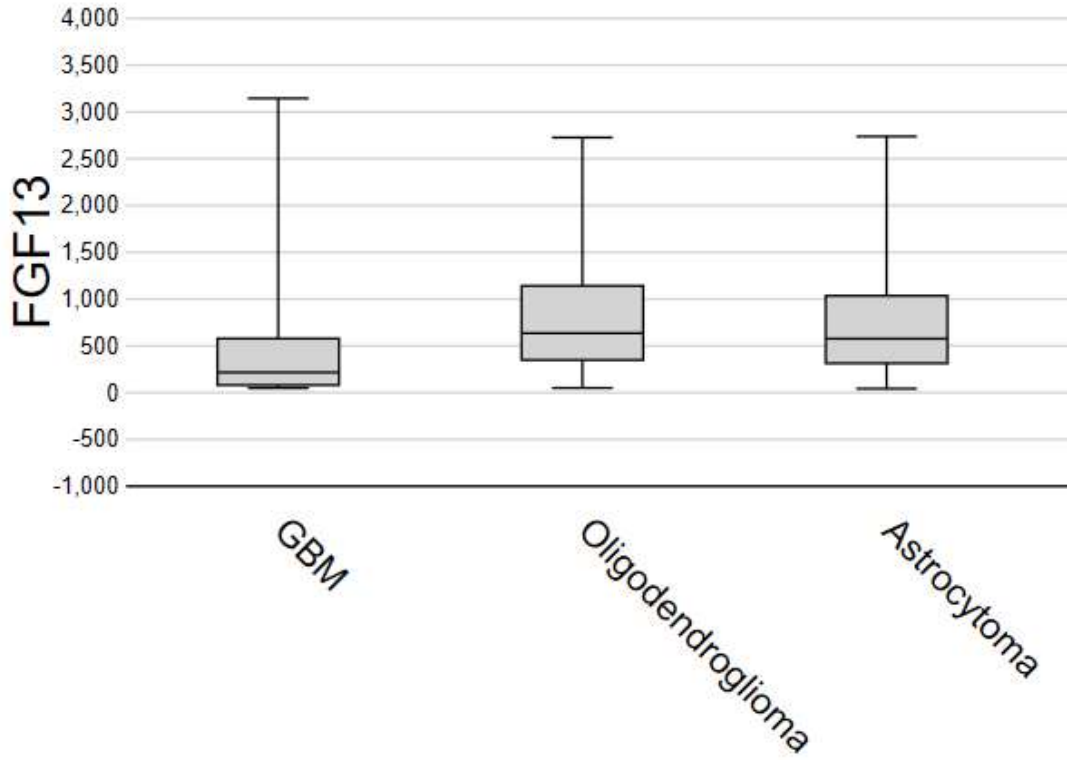

Supplementary Fig. 3
FGF13 expression in glioma subtypes.

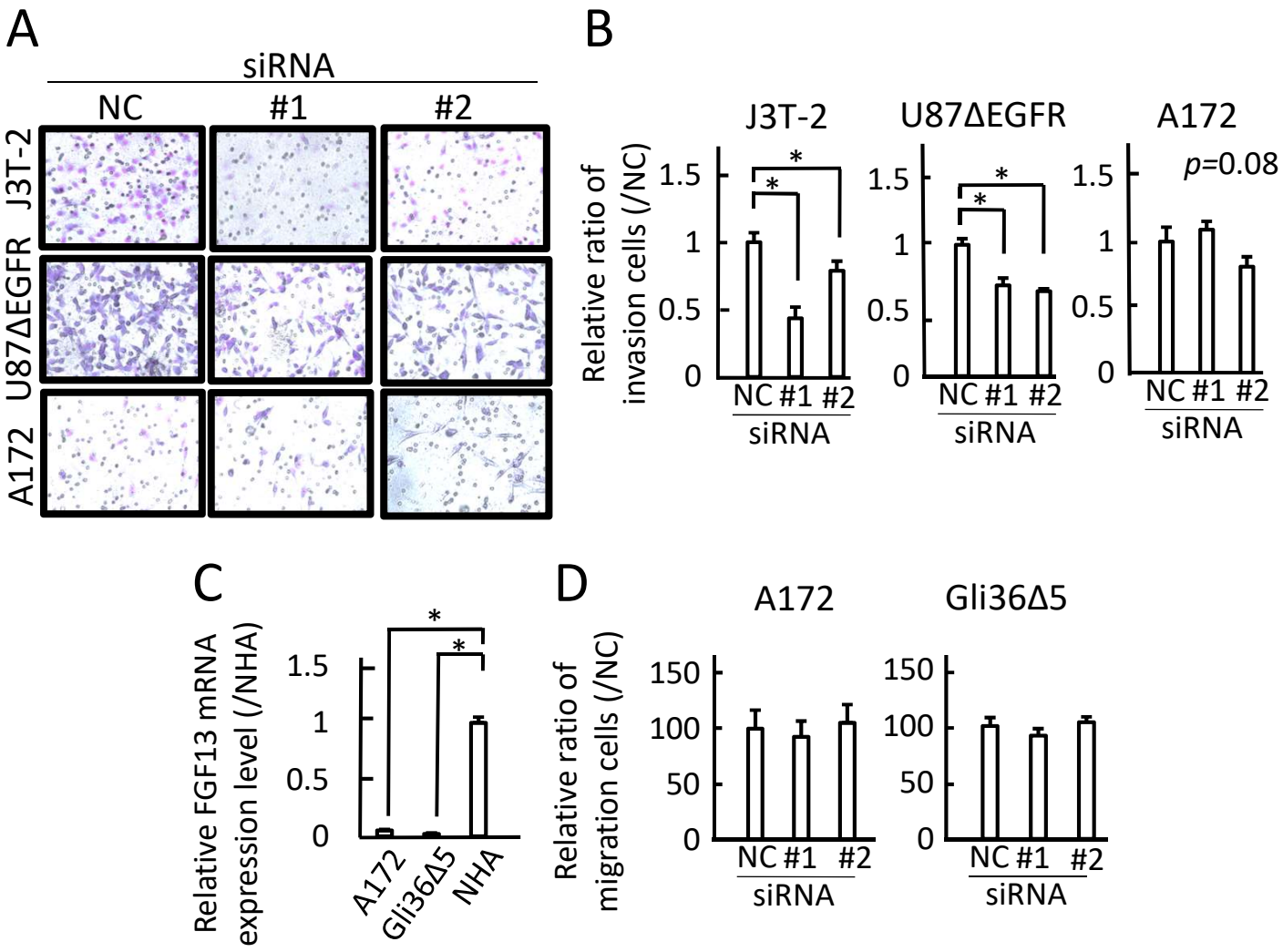

Supplementary Fig. 4

FGF13 was involved in glioma invasion *in vitro*.

(A, B) Knockdown of FGF13 by siRNA decreased the invasion activity of J3T-2 and U87ΔEGFR cells (n=10). In contrast, silencing of FGF13 did not affect the invasion activity of A172 (n=10).

(C) A172 and Gli36Δ5 cell lines expressed very low levels of FGF13 (n=6) compared with that of normal human astrocyte (NHA).

(D) Silencing of FGF13 did not affect the migration activity of A172 and Gli36Δ5 cells.

Data are shown as the mean ± SEM. Statistical significance was calculated by ANOVA with the Dunnett's post hoc test. $^{*}p < 0.05$. NC = negative control siRNA.

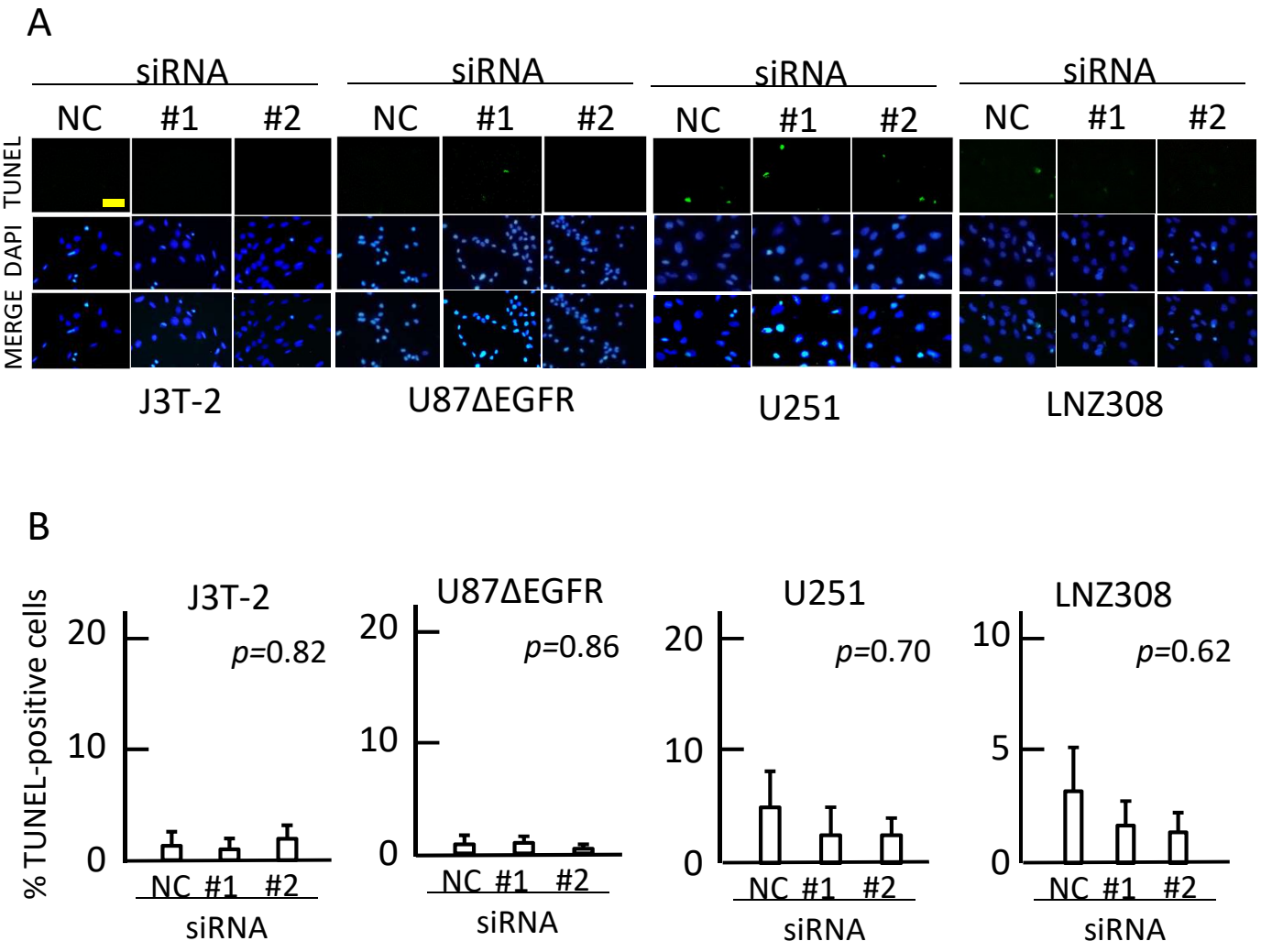

Supplementary Fig. 5

Silencing of FGF13 did not induce apoptosis of glioma cell lines *in vitro*.

(A) Representative pictures from five experiments are shown. TUNEL-positive cells, green; DAPI = 4, 6-diamidino-2-phenylindole, blue. Bar = 50 µm.

(B) Silencing of FGF13 did not induce apoptosis of glioma cell lines *in vitro*. (n=5)

Statistical significance was calculated by ANOVA with Dunnett's post hoc test.

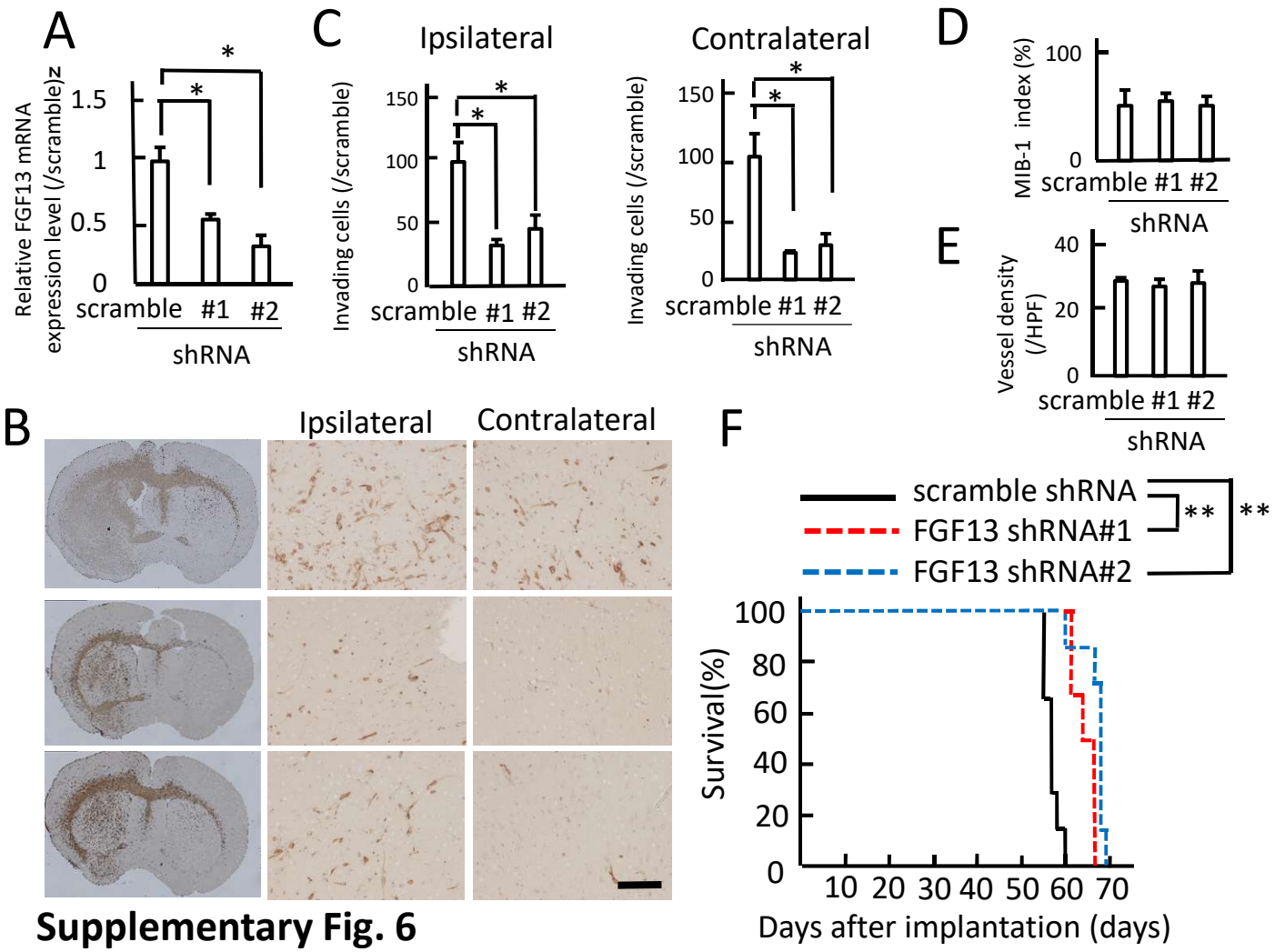

Supplementary Fig. 6

FGF13 was involved in glioma invasion in MGG23 and reduction of FGF13 improved overall survival.

(A) The relative expression level of FGF13 mRNA was decreased by shRNA in MGG23 cells (n = 3).

(B, C) Knockdown of FGF13 in MGG23 impaired glioma invasion as well as MGG8 (n=3). Scale bars, 50 μm.

(D, E) Silencing of FGF13 had no effect on cell proliferation and angiogenesis (n=3).

(D) Kaplan-Meier survival curves of intracranial xenografts with MGG23 cells expressing FGF13 shRNA#1, FGF13 shRNA#2, or scramble shRNA. The survival time of MGG23 expressing either FGF13 shRNA#1 or FGF13 shRNA#2 (median survival = 68 or 65.5 days, respectively) were significantly longer than that of scramble shRNA (58days) (n=8).

*$p < 0.01$, **$p < 0.05$

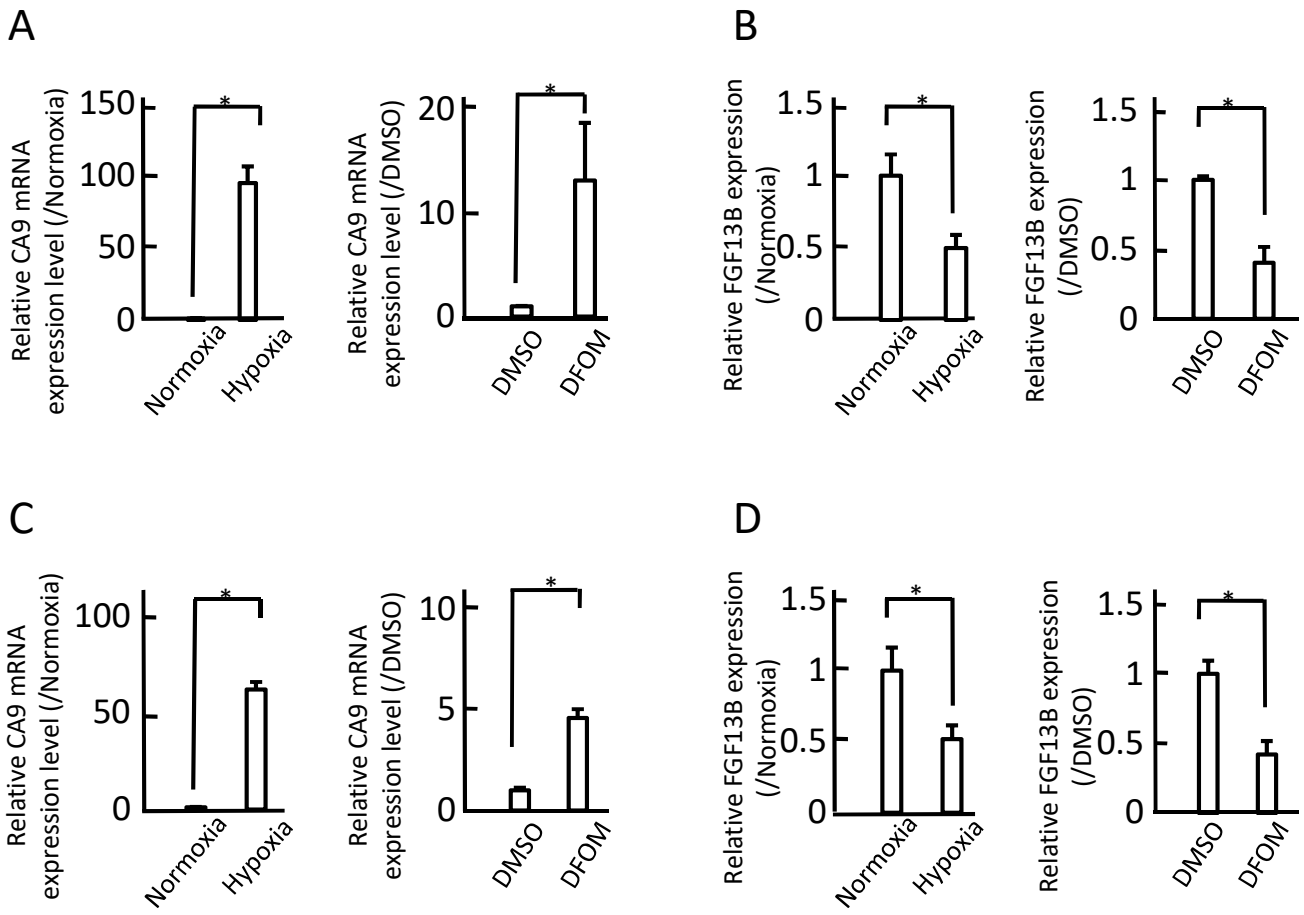

Supplementary Fig. 7

The FGF13 expression was negatively regulated by hypoxia.

(A, C) The relative expression of CA9 mRNA, which is a marker of hypoxic condition, was significantly up-regulated by 1% O_2 (hypoxia) or deferoxamine mesylate (DFMO) in both U87ΔEGFR (A) and U251 (C) (n=3).

(B, D) The relative expression of FGF13B protein was significantly decreased by 1% o2 (hypoxia) or deferoxamine mesylate (DFMO) in both U87ΔEGFR (B) and U251 (D) (n=4).

Data are shown as the mean ± SEM. Statistical significance was calculated by the Student's T-test. $^{*}p < 0.05$.

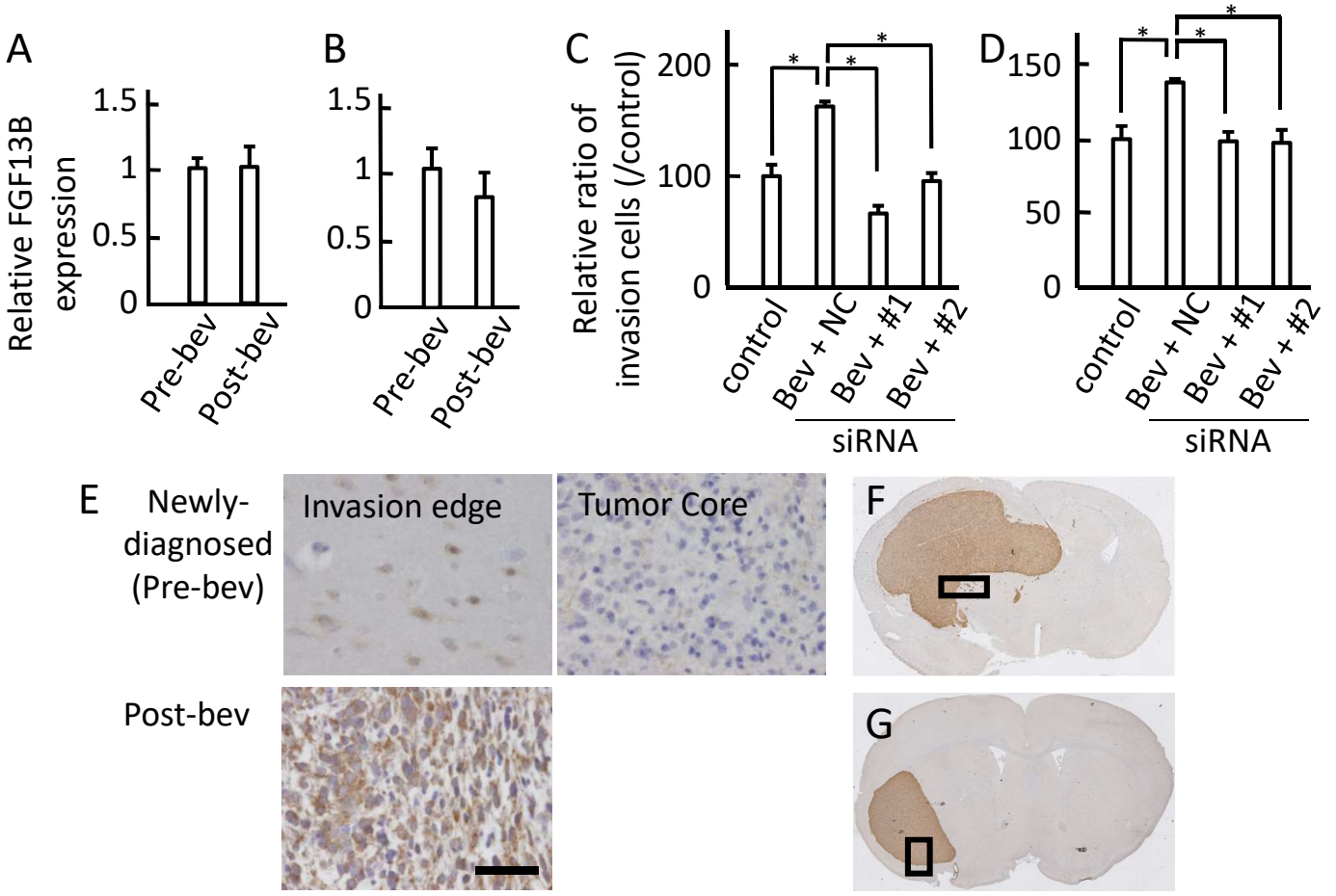

Supplementary Fig. 8

Silencing of FGF13 decreased bevacizumab-induced invasion.

(A, B) Western blotting of U87ΔEGFR (A) and U251 (B) showed that the expression level of FGF13B did not alter after bevacizumab treatment (n=4). Statistical significance was calculated by the Student's T-test.

(C, D) Double chamber assays showed that bevacizumab induced glioma invasion, but silencing of FGF13 inhibited the invasion of U87ΔEGFR (C) and U251 (D) (n=3). Statistical significance was calculated by Tukey's post hoc test. NC = negative control siRNA.

(E) Immunohistochemical staining of a human glioma specimen (case 25) showed FGF13 was expressed after bevacizumab treatment.

(F, G) Immunohistochemical staining of U87ΔEGFR cells transfected with scramble shRNA treated with bevacizumab showed bevacizumab-induced invasion (F). In contrast, silencing of FGF13 decreased the invasiveness (G). The representative results are shown.

Data are shown as the mean ± SEM. $^{*}p < 0.05$.

Fig. 1E

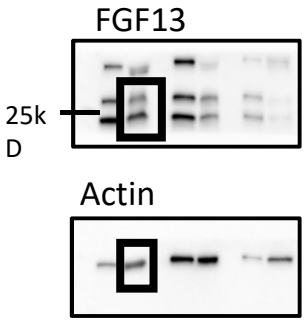

Fig. 2B

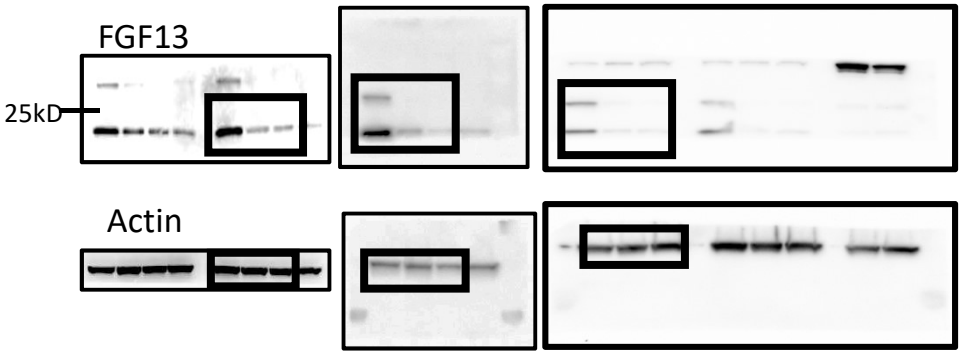

Fig. 5B

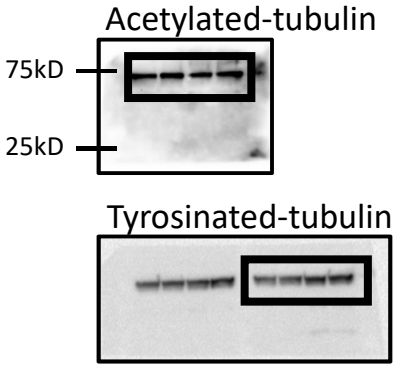

Fig. 5C

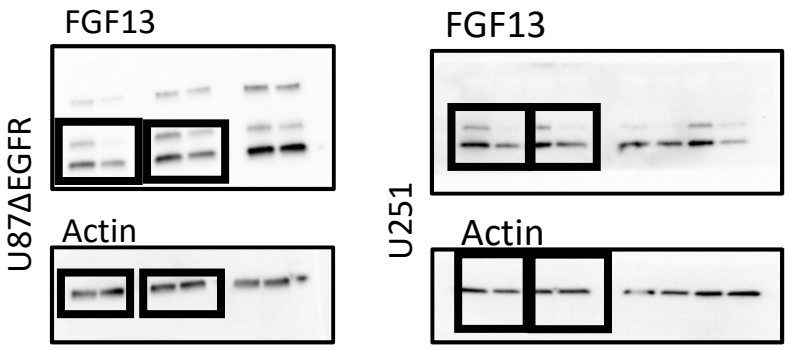

Fig. 6A

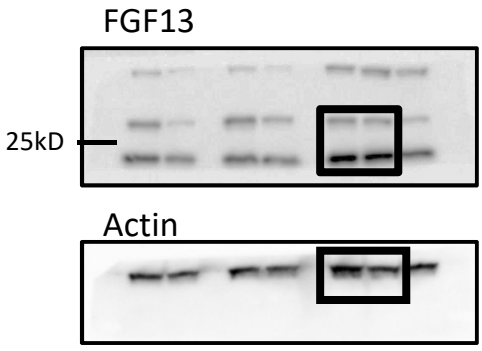

Supplementary Fig. 9

Full scans of the immunoblots shown in the figure. Boxes indicated parts used in the figure and numbers indicated molecular weights.